USGS
science for a changing world

TRANSPORT PATHWAYS IN THE LOWER REACHES OF HOOD CANAL

By

Marlene A. Noble, Anne L. Gartner, Anthony J. Paulson,
Jingping Xu, Edward G. Josberger, and Christopher Curran

2006

Open-File Report 2006-1001

U.S. Department of Interior
U.S. Geological Survey

Transport Pathways in the Lower Reaches of Hood Canal

By

Marlene A. Noble[1], Anne L. Gartner[1], Anthony J. Paulson[2], Jingping Xu[1], Edward G. Josberger[2], and Christopher Curran[2]

Open-File Report 2006-1001

[1]U.S. Geological Survey, Menlo Park, California
[2]U.S. Geological Survey, Tacoma, Washington

INTRODUCTION

In 2003, studies revealed that the waters in the lower reaches of Hood Canal in Washington State have had very low dissolved-oxygen concentrations, low enough to cause some fish kills between June and October of that year.

http://www.hoodcanal.washington.edu/aboutHC/scienceprimer.jsp

Although available data suggests that dissolved-oxygen concentrations have been low in previous years, even as far back as 1950 (Collias et al, 1974), recent measurements have shown that the low dissolved-oxygen conditions have not only become more frequent, but also more persistent.

http://www.hoodcanal.washington.edu/observations/historicalcomparison.jsp

The U.S. Geological Survey's (USGS) Water Resources Discipline (WRD) office in Tacoma, Washington, was asked by Congress to become actively involved in a study of this problem. A meeting between the USGS, local groups and governments, agencies, tribes, and the University of Washington was held on January 8, 2004. It was agreed that the USGS could make a significant contribution to the overall effort to determine the causes and solutions of the low dissolved-oxygen concentrations by assessing the sources and quantifying the amounts of nitrogen compounds discharged by those sources into Hood Canal.

The objectives of assessing nitrogen inputs into Hood Canal will be accomplished in three phases: 1) use available information and data to make initial estimates of the amounts and spatial distribution of nitrogen entering Hood Canal from all sources, 2) use the initial estimates to select, design, and conduct focused studies to better quantify nitrogen loading from major sources to Hood Canal, and 3) use the results of the focused studies to improve the overall estimates of nitrogen loading to Hood Canal.

During phase 1 of the project, one major information gap was identified–the lack of understanding of the transport of nitrogen compounds into Lynch Cove from the rest of the canal, as nitrogen can boost primary production and thus reduce dissolved oxygen. Lynch Cove is at the most landward reach of Hood Canal and is most susceptible to low dissolved-oxygen conditions. In the fall of 2004, the USGS WRD and the USGS Coastal and Marine Geology Team (CMGT) in Menlo Park, California, designed a small, focused research program to assess the currents, density, and oxygen levels in the lower reaches of Hood Canal. This project was designed to provide an initial assessment of the transport of nutrient compounds to Lynch Cove. The data will also be used to model transport processes and oxygen patterns in the canal. This program is part of a larger effort by CMGT to monitor coastal change and coastal ocean processes in the Pacific Northwest. All information collected by this program will be shared with cooperators in the academic and federal communities. In particular, the desired information will be passed to WRD in Tacoma and to the numerical modeling group at the University of Washington. This report describes the data collected in this program and presents an initial analysis of that data.

MOORED ARRAY

A two-month study to obtain information on the circulation patterns and water properties in the lower reaches of Hood Canal was initiated at the end of August 2004 and completed in October 2004 (Figures 1, 2). In order to determine exactly where the moorings should be deployed, a short preliminary cruise was conducted in the lower reaches of the canal to determine the amplitude of the currents and the spatial structures of the current, temperature, and salinity fields. Currents were measured with a shipboard-mounted Acoustic Doppler Current Profiler (ADCP) during a spring tide (Figure 3). A short hydrographic survey determined water properties and oxygen levels in the lower reaches of the canal. ADCPs determine water velocity and channel depth by measuring the return characteristics of acoustic signals using the Doppler shift principle (RD Instruments, 1996). A total of five ADCP transects were measured across Hood Canal at different locations, with start and end points determined using a hand-held GPS receiver. The maximum currents near the surface were about 50 cm/s. Currents near the bed seemed to be much less than 40 cm/s. These current speeds were well within the design limits of the instruments scheduled to be deployed in the canal. There was no marked horizontal shear in the currents along transects near the proposed mooring sites, suggesting that currents measured at the mooring sites would be representative of the regional current field.

After a small bathymetric survey of each proposed deployment location to confirm the suitability of the proposed deployment site, Tripod A (Figure 4) was deployed in the natural constriction at Sister Point and Tripod B was deployed at a nearby location to the west along the canal from the first tripod (Figure 1). Each tripod contained an upward-looking ADCP to collect continuous current data in 1-m bins over the entire water column. Instruments on the tripods also monitored near-bed salinity, temperature, and water clarity (Table 1). In addition, near-bed oxygen was measured at Site B. Each tripod weighed about 1100 pounds. The tripods were deployed for eight weeks to cover at least two lunar cycles. Most instruments sampled the water properties every five minutes.

Mooring A

The tripod at Site A was deployed in 54 m of water. The first bin in the upward-looking ADCP at Site A was centered in water depth of 47.3 m, about 7 m above bed (mab). The last surface bin that contained high-quality data was centered around 3.3 m below the surface. A Microcat was attached at 59 cm above bed (cmab) to measure conductivity and temperature. Two Brancker loggers were attached with transmissometers to measure temperature and near-bottom water clarity (Figure 5a).

Mooring B

The tripod at Site B was deployed in 44 m of water. The first bin in the upward-looking ADCP at Site B was centered in water depth of 37.9 m, about 6 mab. The top bin measured currents centered around 3.9 m from the surface. A Microcat was attached at 53 cmab to measure conductivity and temperature. Two Brancker loggers were attached with transmissometers to measure temperature and near-bottom water clarity. A Seacat measured near-bottom oxygen concentrations at 90 cmab, as well as temperature and salinity at 64 cmab (Figure 5b).

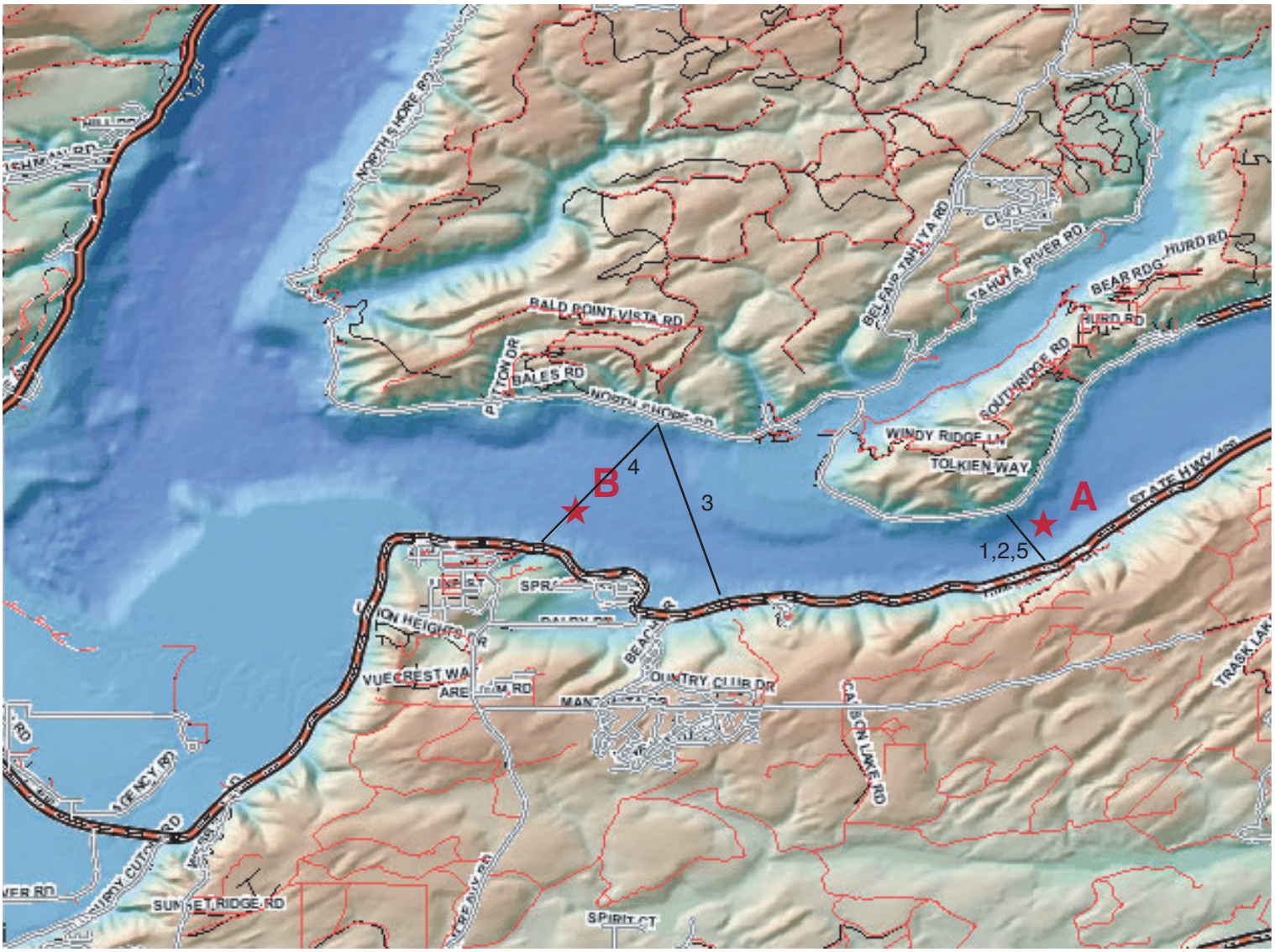

Figure 1. Location of mooring sites in Hood Canal and index map. Black lines (1-5) show approximate locations of transect lines from Figure 3.

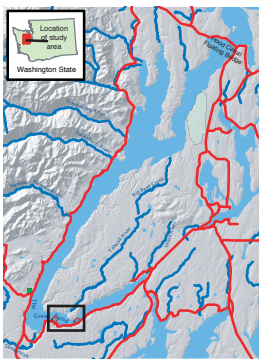

Study area →

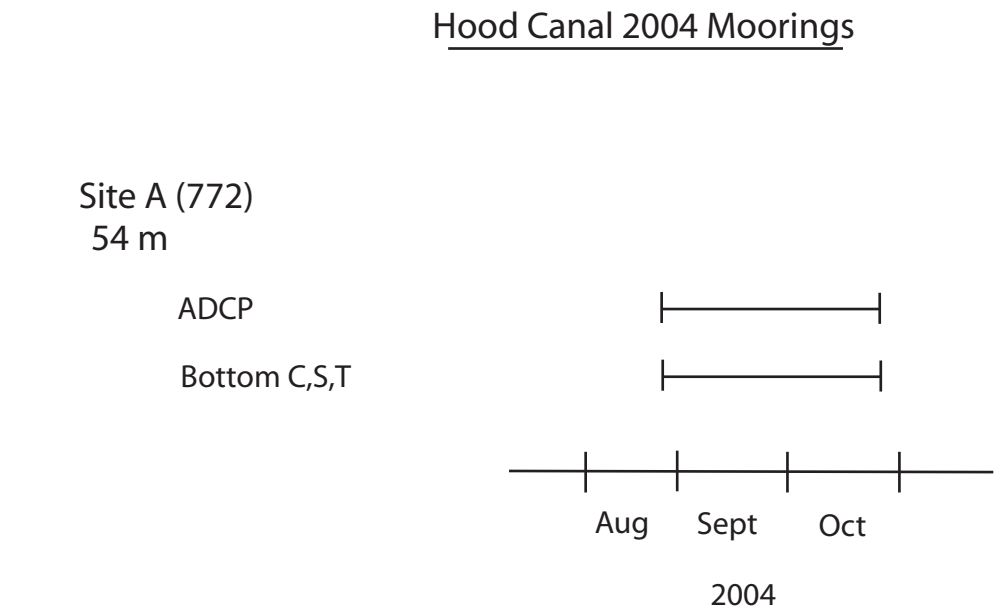

Figure 2. Timelines showing dates when valid data from current meters and data for temperature, water clarity, oxygen, and salinity exist for Hood Canal sites.

Transect #1

Start time: 0916 PDT	Location: N 47 21’ 20”	W 123 01’ 07”
End time: 0929	End loc. N 47 21’ 39”	W 123 01’ 28”

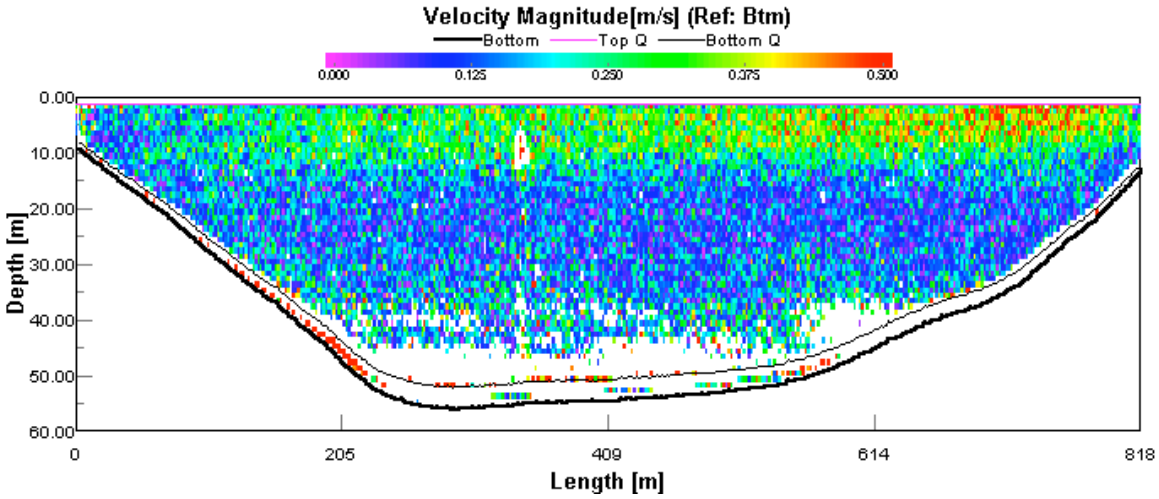

Transect #2

Start time: 1004 PDT	Location: N 47 21’ 39”	W 123 01’ 28”
End time: 1017	End loc. N 47 21’ 20”	W 123 01’ 07”

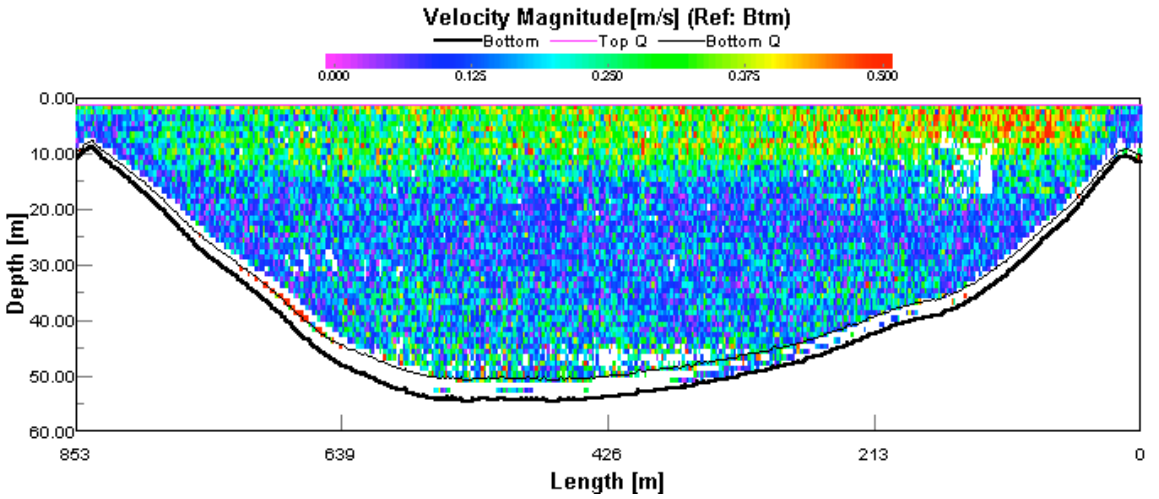

Figure 3. Transects taken in short preliminary cruise with ACDP to measure currents. See Figure 1 for location of transect lines.

Transect #3

Start time: 1037 PDT	Location: N 47 20’ 59”	W 123 03’ 36”
End time: 1108	End loc. N 47 22’ 16”	W 123 03’ 59”

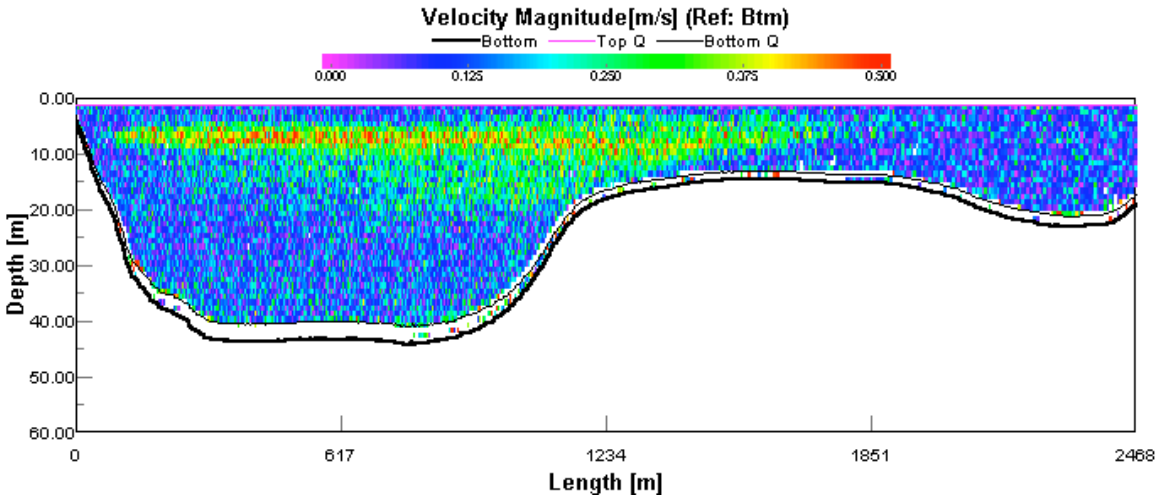

Transect #4

Start time: 1116 PDT	Location: due SW of Transect#3 end point	
End time: 1136	End loc. N 47 21’ 26”	W 123 05’ 20”

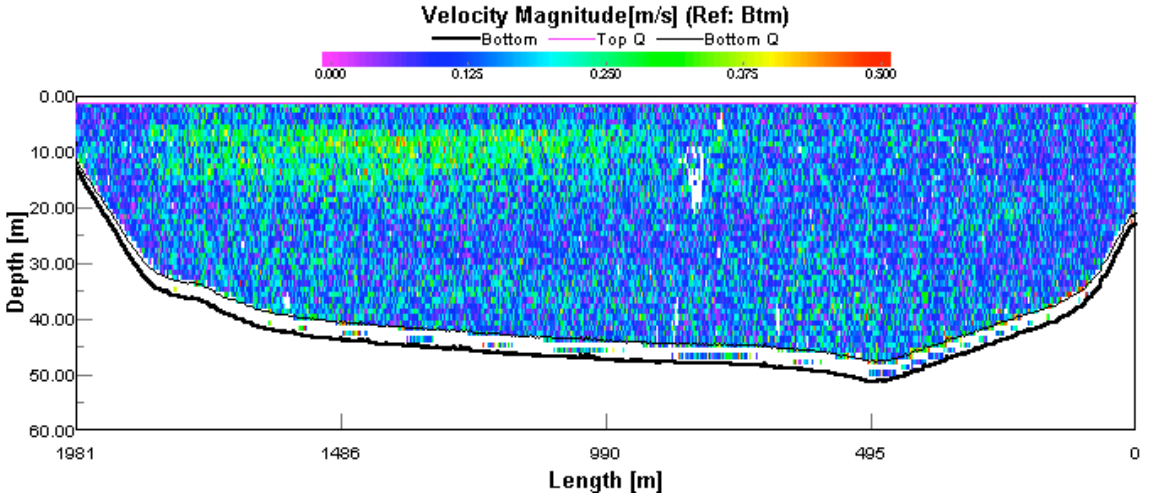

Figure 3, cont.

Transect #5

Start time: 1227 PDT	Location:	N 47 21’ 39”	W 123 01’ 28”
End time: 1237	End loc.	N 47 21’ 20”	W 123 01’ 07”

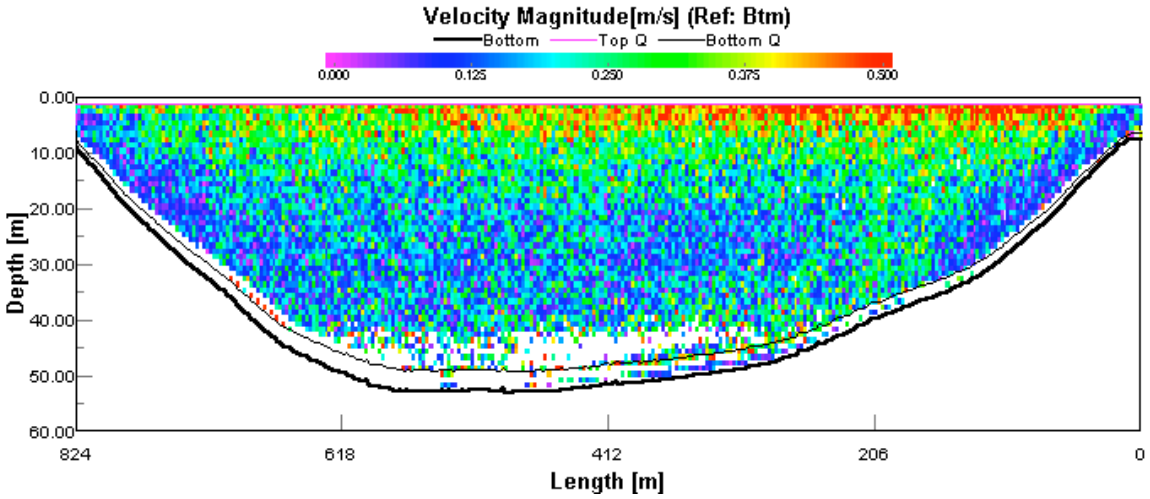

Figure 3, cont.

Table 1. Data availability for Sites A and B tripods.

USGS Cruise ID #	Location		Deployment date	Recovery date	Water depth (m)	Instrument Type	Manufacturer and Model #	Instrument depth (cmab)	Variables Measured	Sampling Rate	Serial Number
	Latitude	Longitude									
7721	47°21.51 N	123°01.14 W	8/28/04	10/28/04	54	300kHz ADCP	RDI Instruments Workhorse Sentinel	122	V	5 min	587
7722						Microcat	SBE 37-5M	59	T,S	5 min	2538
						Brancker	XR-420	104	L	5 min	10750
7723						Transmissometer	Seatech TR2025	104	Clarity	5 min	21
						Brancker	XR-420	49	L	5 min	10752
7724						Transmissometer	Seatech TR2025	49	Clarity	5 min	515
7731	47°21.75 N	123°04.81 W	8/26/04	10/26/04	44	300kHz ADCP	RDI Instruments Workhorse Sentinel	122	V	5 min	411
7732						Seacat	SBE 16+	64	T,S	5 min	4250
						Oxygen sensor	Seabird 43	64	Oxygen	5 min	430253
7733						Microcat	SBE 16+	53	T,S	1 min	283
						Brancker	XR-420	103	L	5 min	10754
7734						Transmissometer	Seatech TR2025	103	Clarity	5 min	516
						Brancker	XR-420	48.5	L	5 min	10755
7735						Transmissometer	Seatech TR2025	48.5	Clarity	5 min	618

Figure 4. Recovery of Tripod A in October 2004.

While the moorings were in the water, several casts with a conductivity-temperature-depth (CTD) sensor that measured the temperature and salinity of the water column were taken near the instrument sites (Figures 6a-d). In addition, nutrients and other ancillary constituents within Lynch Cove were discretely sampled several times during the deployment period in order to collect the chemical data needed to calculate the transport of nutrients into Lynch Cove from the seaward reaches of Hood Canal.

DATA QUALITY AND PROCESSING PROCEDURES

The data sets from individual instruments were downloaded, transcribed into scientific units, and then passed through several quality-control steps. The data were checked for errors caused by instrument failures. Obvious spikes and gaps were removed from the data. Greenwich mean time (GMT) is the common timebase for all data records.

There were short temporal gaps in many of the data records. Most gaps were less than 10 minutes long. Gaps of less than 20 minutes were linearly interpolated. Gaps of a few hours were filled with a spectral method that uses the frequency properties of the data adjacent to the gap to generate the interpolated data. Longer gaps were not filled.

The very-near surface currents measured by the ADCPs were removed from the current-meter files due to obvious measurement errors. Hence, the shallowest currents measured at Sites A and B were 3.3 and 3.9 m below the surface at the lowest portion of the tidal cycle. The

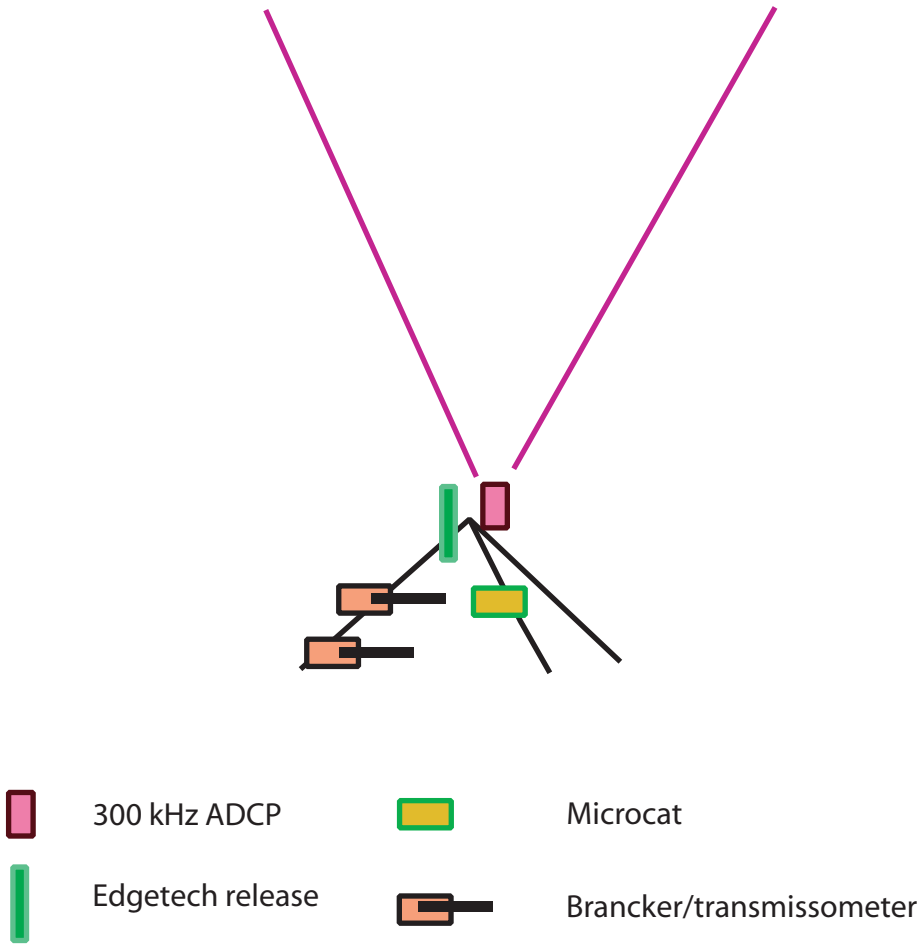

Figure 5a. Schematic diagram of tripod mooring at 54 m at Site A.

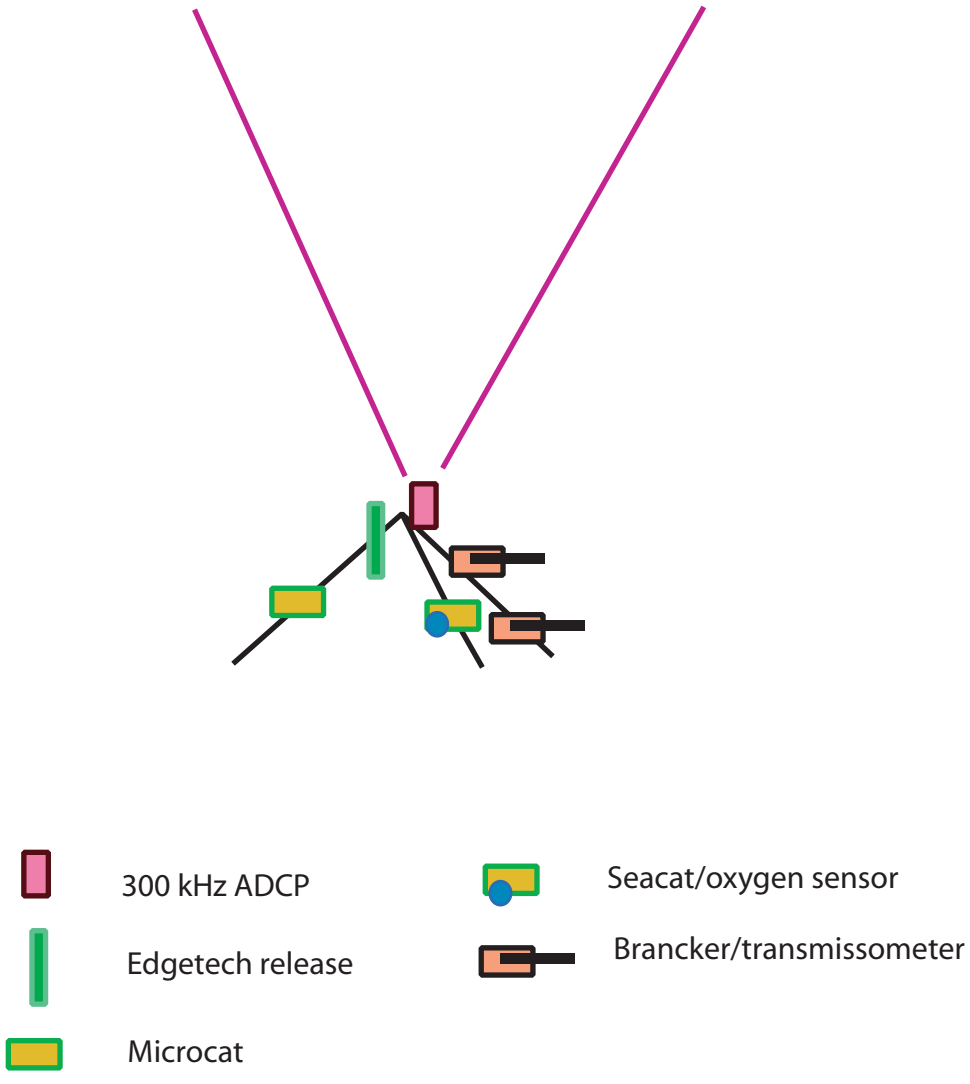

Figure 5b. Schematic diagram of tripod mooring at 44 m at Site B.

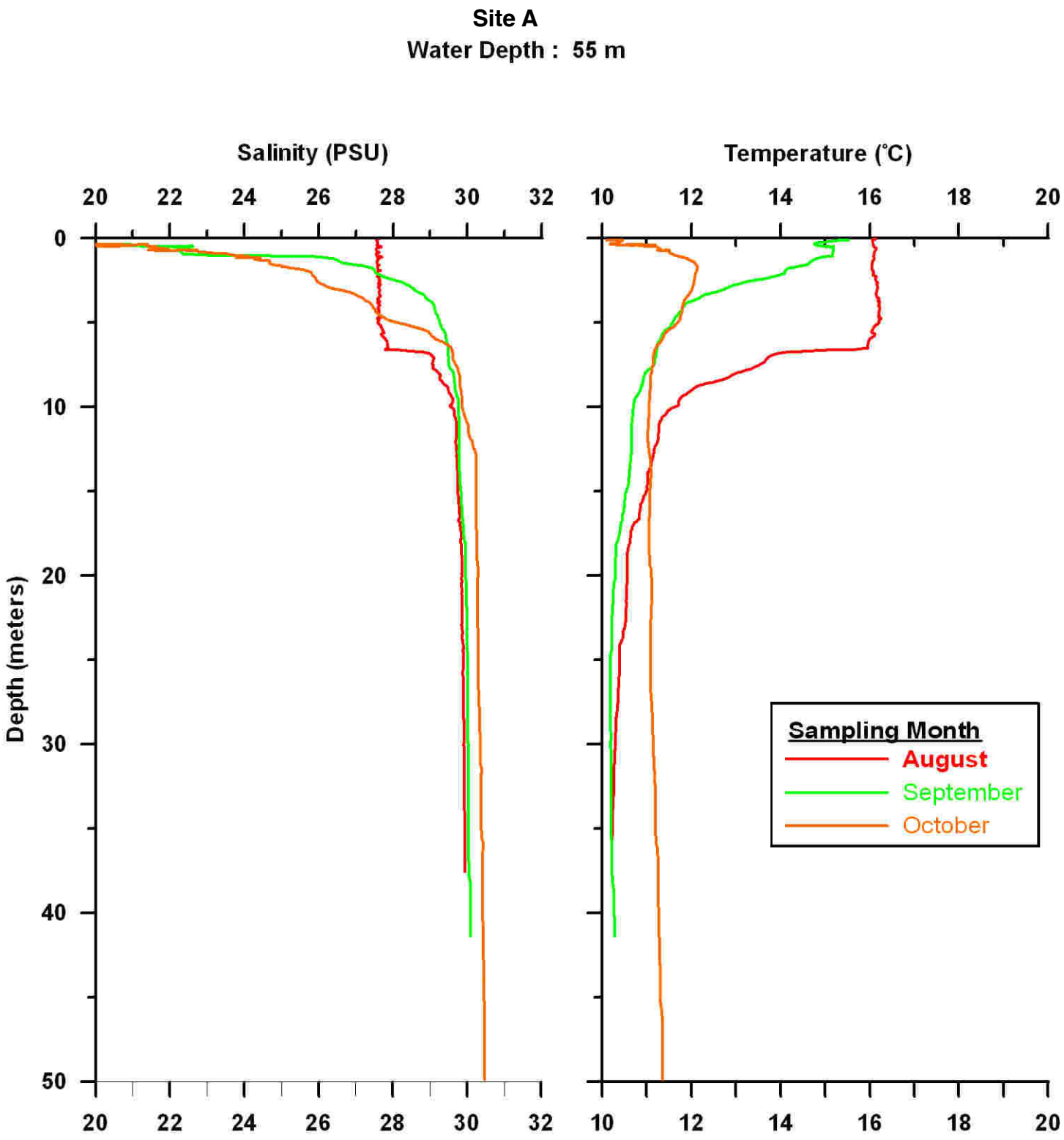

Figure 6a. Water column temperature and salinity profiles recorded by CTD casts taken near Site A.

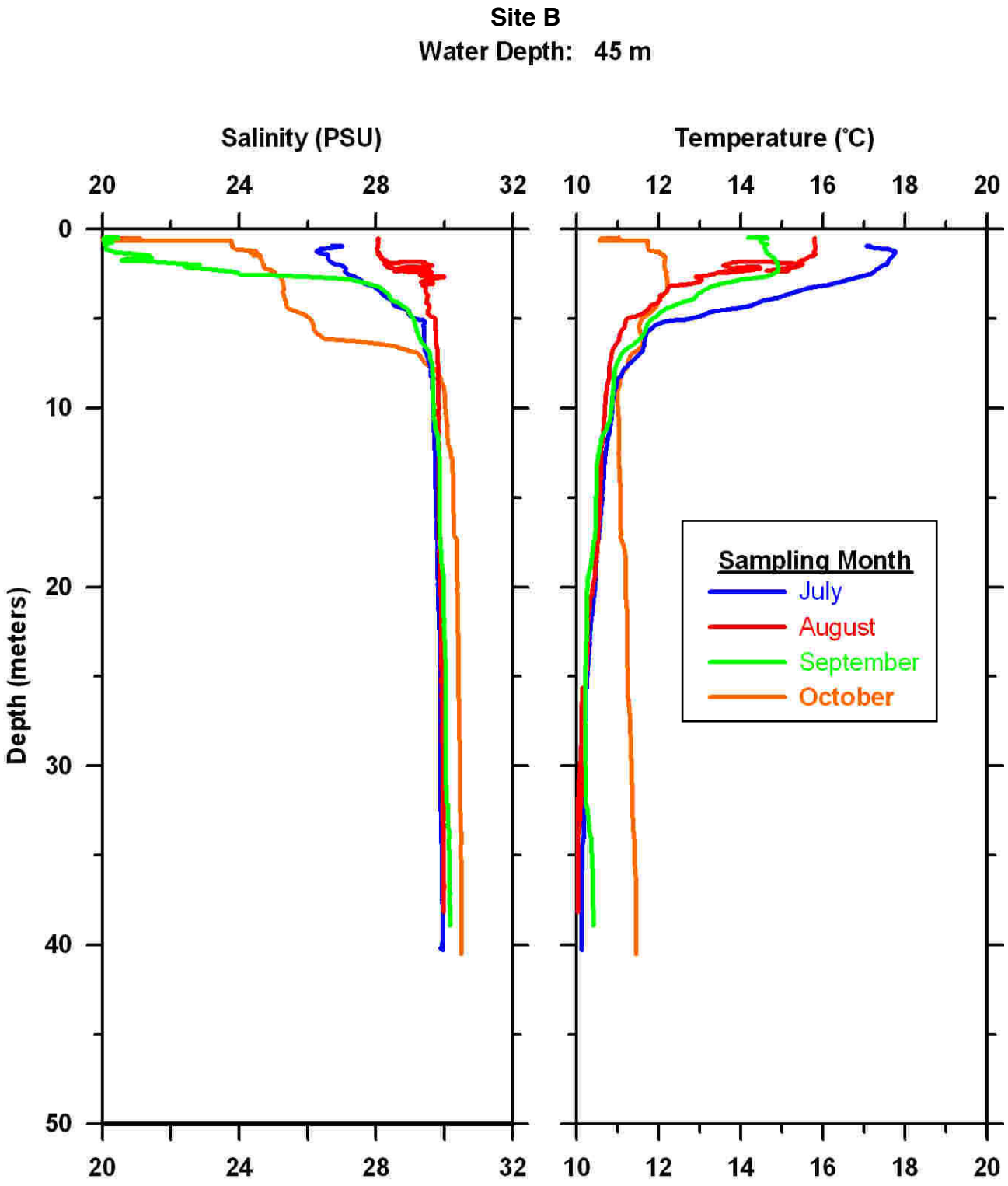

Figure 6b. Water column temperature and salinity profiles recorded by CTD casts taken near Site B.

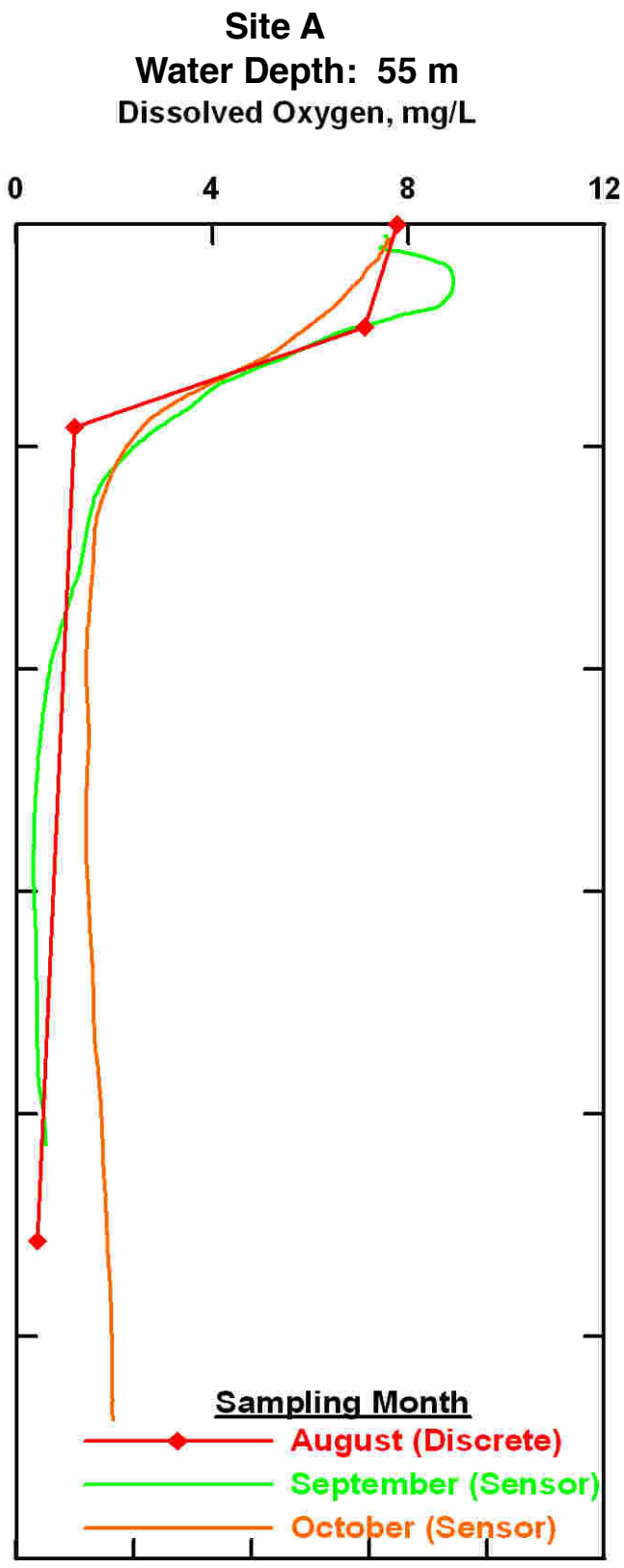

Figure 6c. Water column temperature and salinity profiles recorded by CTD casts taken near Site A.

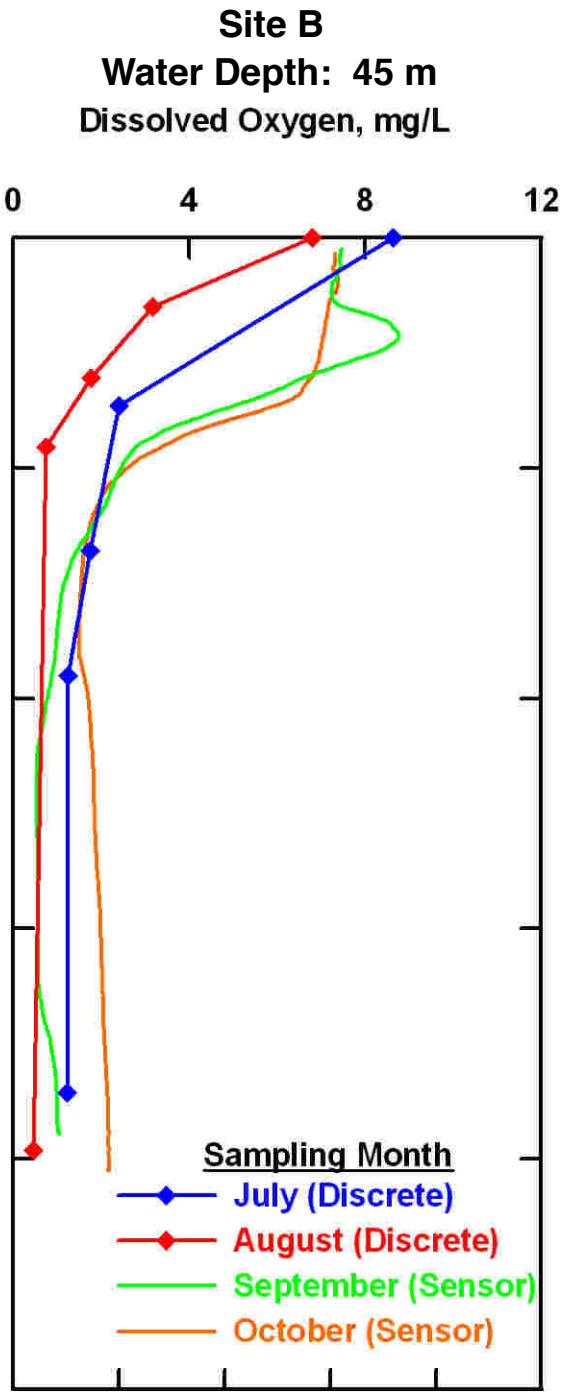

Figure 6d. Water column temperature and salinity profiles recorded by CTD casts taken near Site B.

deepest currents measured at these sites were in water depths of 47.3 and 37.9 m, which was about 6-7 mab.

The currents at Sites A and B were rotated into a coordinate system aligned roughly parallel and perpendicular to the local axis of the canal. At Site A, positive along-canal currents flow toward the mouth (seaward), aligned toward 225 degrees true. Positive cross-canal currents flow toward the northwest shore, aligned toward 315 degrees. The positive along-canal currents at Site B are aligned toward 295 degrees. They also flow toward the mouth (seaward) of the canal. Positive cross-canal currents are aligned along 25 degrees, flowing toward the northern shore.

Several statistical quantities are discussed in this report. The mean, standard deviation, and minimum and maximum amplitude of many measured water properties are included in Appendix A (Tables A-1a, A-1b). The error bars around the mean values indicate the stability of that mean value. In order for a mean current direction to be reliable, the mean values must be greater than the error bar. Otherwise, the mean directions are not significantly different from zero.

The formula for the error bar around the mean is

$$\frac{\sigma t_{n;\alpha/2}}{\sqrt{n+1}} \qquad (1)$$

where σ is the standard deviation of the subtidal data, t is the student t statistic at the 100(1-α) percent confidence limit, and (n+1) is the degrees of freedom in that data. The degrees of freedom is the record length divided by the auto-correlation scale of the subtidal data set. For currents, there were 19 degrees of freedom.

The tidal analysis is the result of performing a least-squares fit of the observed series to amplitudes and phases of specific frequencies that are derived from the motions of the sun and moon. The methods are given in Godin (1972), and the implementation for the pressure and current records uses the programs written by Foreman (1977; 1978). The major constituents of interest are grouped into two frequency bands, the semidiurnal (M_2, S_2) and diurnal (K_1, O_1). Tidal current amplitudes were computed for currents measured each meter for water depths 6-7 m above the seabed and 3-4 m below the estuary's surface. A barotropic, or surface, tide was calculated from currents averaged over the entire water column.

The current records were also low-pass filtered to remove the diurnal and semidiurnal tidal constituents from the records. These records are designated subtidal currents.

MOORED CURRENT OBSERVATIONS

Mean currents

All current components–mean, tidal, and subtidal currents–are generally aligned with the axis of the canal. The mean currents for the two-month measurement period were generally weak. At Site B, the mean along-canal flow was not significantly different from zero (Appendix A; Table A-1b). At Site A, the mean along-canal current was slightly stronger at depths deeper than 34 m. At these depths, average currents flowed about -1.94 $\pm$ 1.44 cm/s landward, toward the head of the canal (Appendix A; Table A-1a).

Tidal current and sea-level fluctuations

Tidal currents are a major portion of the current field in Hood Canal. The semidiurnal tidal currents (primarily M_2 and S_2) flow up and down the canal roughly twice per day. The diurnal tidal currents (primarily O_1 and K_1) flow up and down the canal once a day. The depth-averaged (or barotropic) tidal current is aligned with the axis of Hood Canal (Appendix A; Table A-2). The principal lunar component of the barotropic tide (M_2) is the dominant tidal current. Maximum along-canal M_2 current amplitudes were 8 and 14 cm/s at Sites B and A respectively. The along-canal currents associated with the other three barotropic tidal components were generally weak, 5 cm/s or smaller at both sites. Usually, the along-canal tidal currents at Site A were twice the size of tidal currents measured at Site B. This is consistent with canal topography. The cross-sectional area of the canal at Site A is only half that measured at Site B; hence currents must flow faster through this relatively narrow portion of the canal. The phase change in tidal currents between the two sites was minimal. The cross-canal tidal currents, as represented by the amplitude of the minor axis of the tidal current ellipse, were at least an order of magnitude smaller than the along-canal currents.

The detailed measurements of velocity with depth in Hood Canal showed that, although the depth-averaged tidal currents accounted for most of the tidal flow, there was some vertical structure in the amplitude and the phase of tidal currents at both sites (Appendix A; Tables A-3a-d, A-4a-d). At each depth level, the measured along-canal tidal currents were usually only 20 percent larger or smaller than the depth-averaged tidal current. The phases of each tidal constituent were fairly steady over the water column and close to the phases of their respective barotropic constituent.

The sea-level fluctuations associated with the diurnal and semidiurnal tides were 0.5 to 1 decibar (approximately 0.5-1 m) (Appendix A; Table A-2). The amplitude of the sea-level (or pressure) fluctuation for each tidal constituent was nearly identical at both sites. There was no significant change in the tidal phase between Sites A and B.

Within the diurnal and semidiurnal tidal bands, the barotropic tidal currents and sea-level fluctuations have similar ratios for their relative amplitudes. The ratio of K_1 to O_1 amplitudes is approximately 1.5 for both currents and sea level. The ratio for M_2 to S_2 is 3. The diurnal ratio is what one would expect from simple astronomical tidal forcing. The ratio of the semidiurnal components is somewhat larger, indicating M_2 is slightly larger (or S_2 is slightly smaller) than one would expect from astronomical forcing. The phase shift between the barotropic tidal currents and sea level is around 110° for the diurnal constituents and 125° for the semidiurnal constituents. The phase properties suggest that the tidal currents are nearly, but not quite, a standing wave, as the phase is slightly larger than 90°.

Subtidal current patterns

The vertically averaged subtidal currents at Sites A and B flow primarily up and down the canal (Figure 7). Most of the energy in the fluctuating flow showed periods between 3 and 6 days. There is a slight tendency for the flow at Site A to be towards Lynch Cove, at the head of the canal, with speeds of 1 cm/s (Table 2). It is clear that the amplitude of the fluctuations in the along-canal flow at Site A is twice that measured at Site B, consistent with the changes in the cross-sectional area of Hood Canal at these two sites. It is also obvious that the flow up and

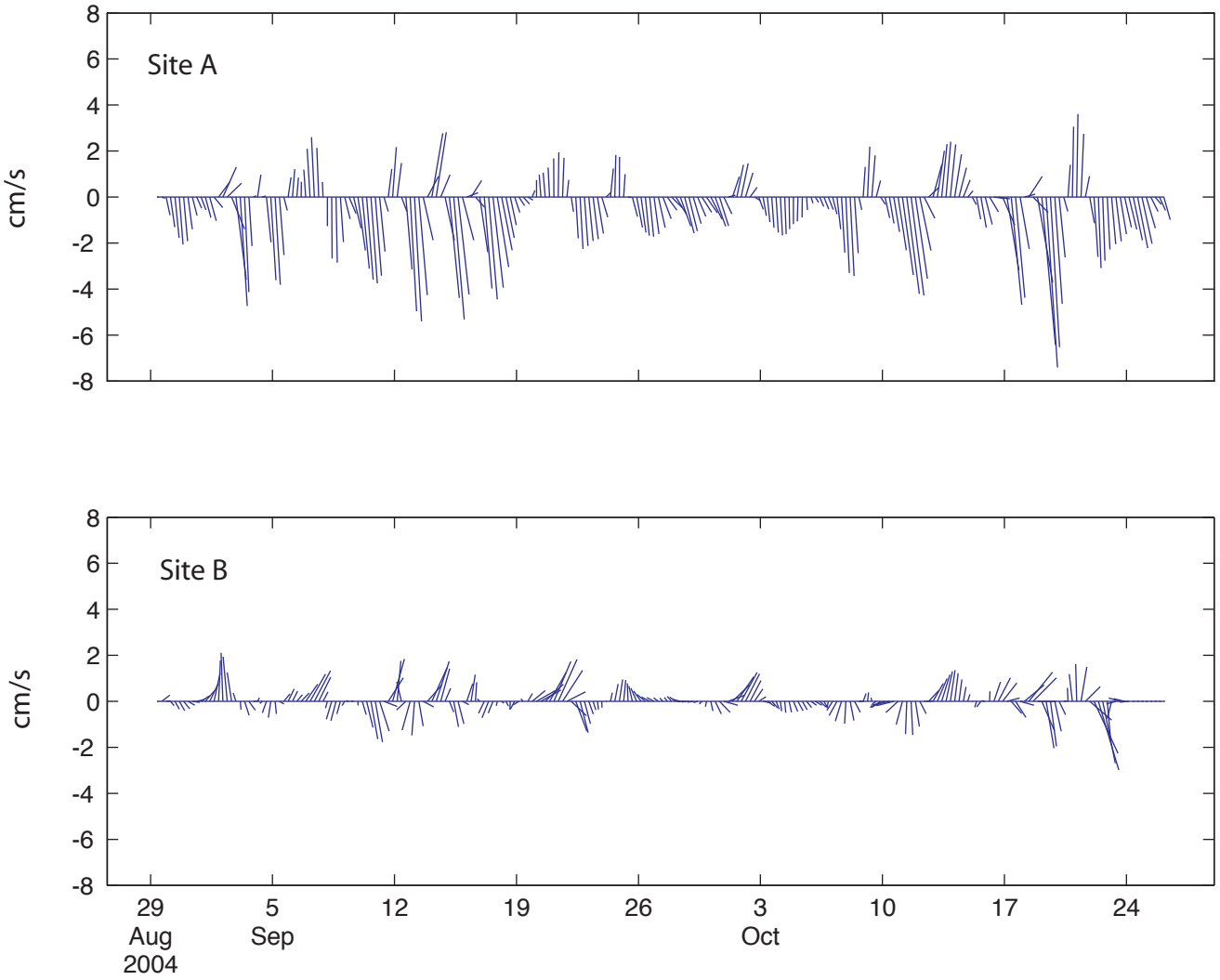

Figure 7. Subtidal currents summed over the water column. The length of each line in the plot indicates the speed of the subtidal flow. The angle of each line represents the direction of flow. Hence a positive vertical line indicates currents are flowing parallel to the canal axis toward the mouth of Hood Canal.

Table 2. Statistics for vertically averaged along-canal currents. The currents are averaged over the entire water column (VA) or over the surface (SF) and lower layer (LL) of the water column as defined by the first mode in the current field for Sites A and B. Mean currents are significant at the 95 percent confidence level.

Site	Mean (cm/s)	Standard Deviation
VA_A	-1.0	1.9
VA_B	0	0.9
SF_A	0	3.8
LL_A	0	2.7
SF_B	0	2.7
Ll_B	0	1.7

Table 3. Coherence for various pairs of subtidal currents in the 3-6-day frequency band. The currents are averaged over the entire water column (VA) or over the surface (SF) and lower layer (LL) of the water column as defined by the first mode in the current field for Sites A and B. Reported coherences are significant at the 95 percent confidence level. A transfer function (Tr) larger than 1 means that the coherent portion of the energy in the second pair is larger that that in the first. Phases of 0 and 180 are reported if the measured phase is not significantly different from those values. The lowest resolvable period was 444 hours.

Current 1	Current 2	Coherence	Phase	Tr
VA_B	VA_A	0.89	0	2.2
VA_A	LL_A	0.97	0	1.4
VA_B	LL_B	0.80	0	2.0
SF_B	SF_A	0.95	0	1.3
LL_B	LL_A	0.92	0	1.3
SF_A	LL_A	0.78	180	0.6
SF_B	LL_B	0.80	180	0.6
Mode_2 B	Mode_2 A	0.64	0	1.0

down the canal is highly correlated between sites. The coherent (or similar) portion of the fluctuating flow field in the 3-6-day band accounts for 79 percent of the energy (Table 3).

However, if one examines only vertically averaged current records, one misses the fact that there is a persistent vertical structure in the subtidal current field. Currents near the surface tended to flow in opposite directions to currents near the bed (Figure 8). The change in flow direction occurred below the relatively shallow thermocline at a depth of 10 m (Figures 6a-d). Because the flows in each layer (surface and bottom) were highly correlated both within and between layers, Empirical Orthogonal Functions (EOF) (Joreskog et al, 1976) were used to represent this vertically sheared current field. The first mode of an EOF represents the most energetic spatial pattern associated with the correlated portion of a fluctuating current field. The first mode represents both the amplitude variation and the temporal fluctuations in a set of currents in a particular region if that mode contains a large percentage of the variance, or energy, in the regional current field. The second mode represents the next most energetic correlated structure in that current field.

The vertical structure of subtidal currents in the first mode confirms the initial observation that the majority of currents above the thermocline flow in a direction opposite to currents below the thermocline (Figure 9).

At Site A, the first mode accounts for 75 percent of the subtidal along-canal flow (Table 4a). The surface layer is quite shallow, extending to only 6 m of water depth. The lower layer is much thicker, extending from about 13 m below the surface to the bed. There is a similar sheared flow pattern at Site B, where the first mode accounts for 63 percent of the flow field. The surface layer at Site B is 5 m deeper than that found at Site A. This may relate to the changing depth of the thermocline at the two sites, as there is a slight tendency for the thermocline to be deeper in September and October at Site B (Figure 6b).

In order to examine the sheared flow pattern more closely, subtidal along-canal currents in the surface and lower layer at each site were averaged over the bins defined by the mode (Table 4a). The currents in the two layers clearly flow in opposite directions (Figure 10). Not surprisingly, the coherence between the surface and lower layers is 0.8, with a phase of 180 degrees (Table 3; Figure 10).

Fluctuations in the averaged along-canal currents ranged from 5-10 cm/s (Figure 10). These current oscillations can transport suspended material more than 15 km in a few days. Currents in the lower layer are not quite as strong as those in the surface layer, but because the lower layer is much thicker, they dominate the net transport. Hence, the currents averaged over the entire water column not only flow in the same direction as in the lower layer, but also are highly coherent with the lower layer currents at both sites (Table 3). Eighty to ninety percent of the vertically averaged fluctuating flow field at Site A is represented by flow below the thermocline.

When currents in the surface layer at Site A are flowing toward the mouth (seaward) of the canal, surface currents at Site B are slower, but flowing in the same direction (Figure 11). Currents in the lower layer at both sites are flowing toward the head of the estuary. Flows in both the surface and lower layers are highly coherent between measurement sites; coherence amplitudes are above 0.9 (Table 3; Figure 11). There was no measurable phase lag between the two sites.

The high correlations in modal currents between Sites A and B suggest that the vertically sheared fluctuating flow field has a length scale much larger than the 5-km separation of the two measurement sites. A simple calculation using Merian's formula (Pond and Pickard, 1983) for the length-scale of an internal seiche with periods of 3-6 days suggests that the seiche could

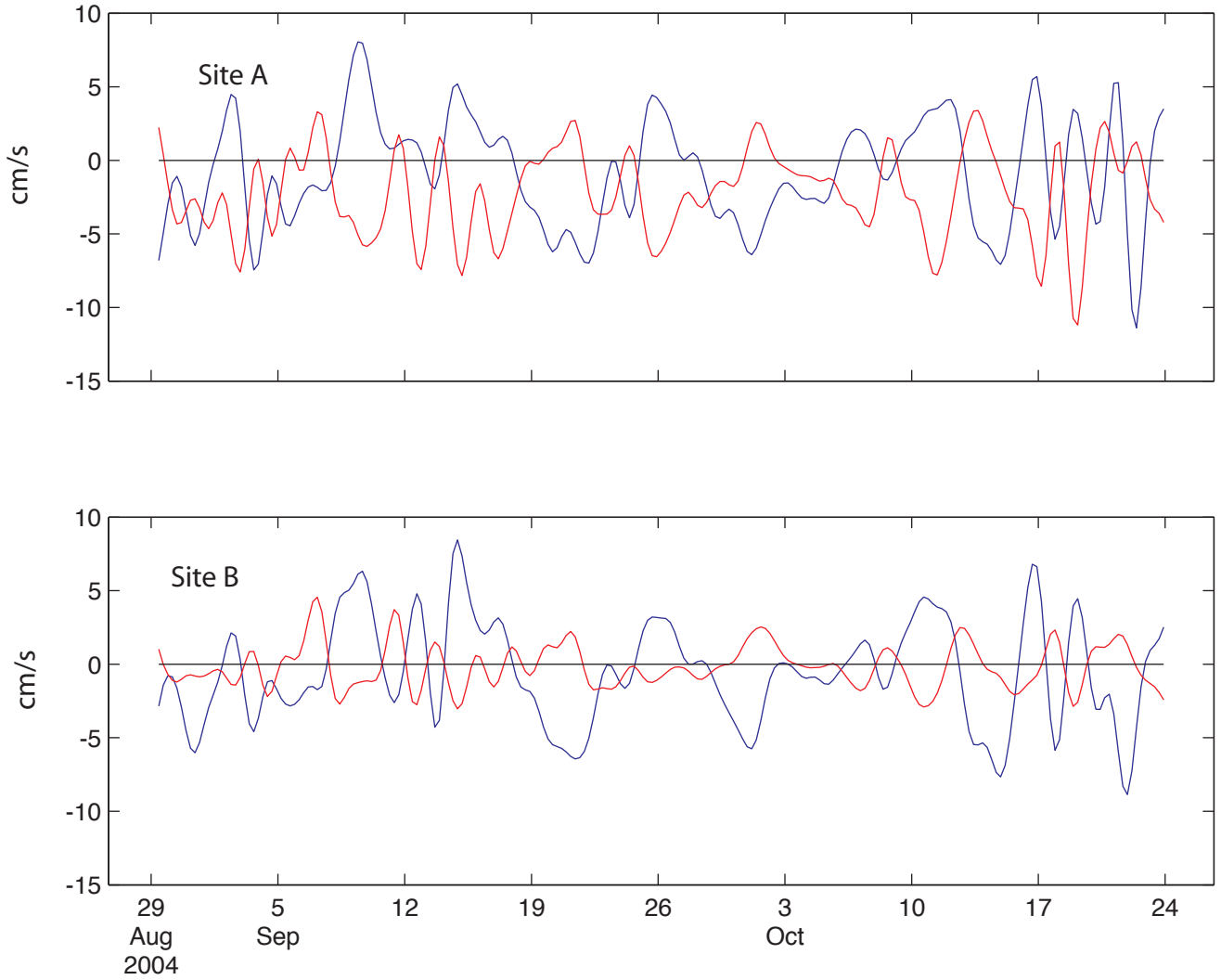

Figure 8. Subtidal currents nearly 6 m below the surface (blue) and 9 m above the bed (red) at Sites A and B.

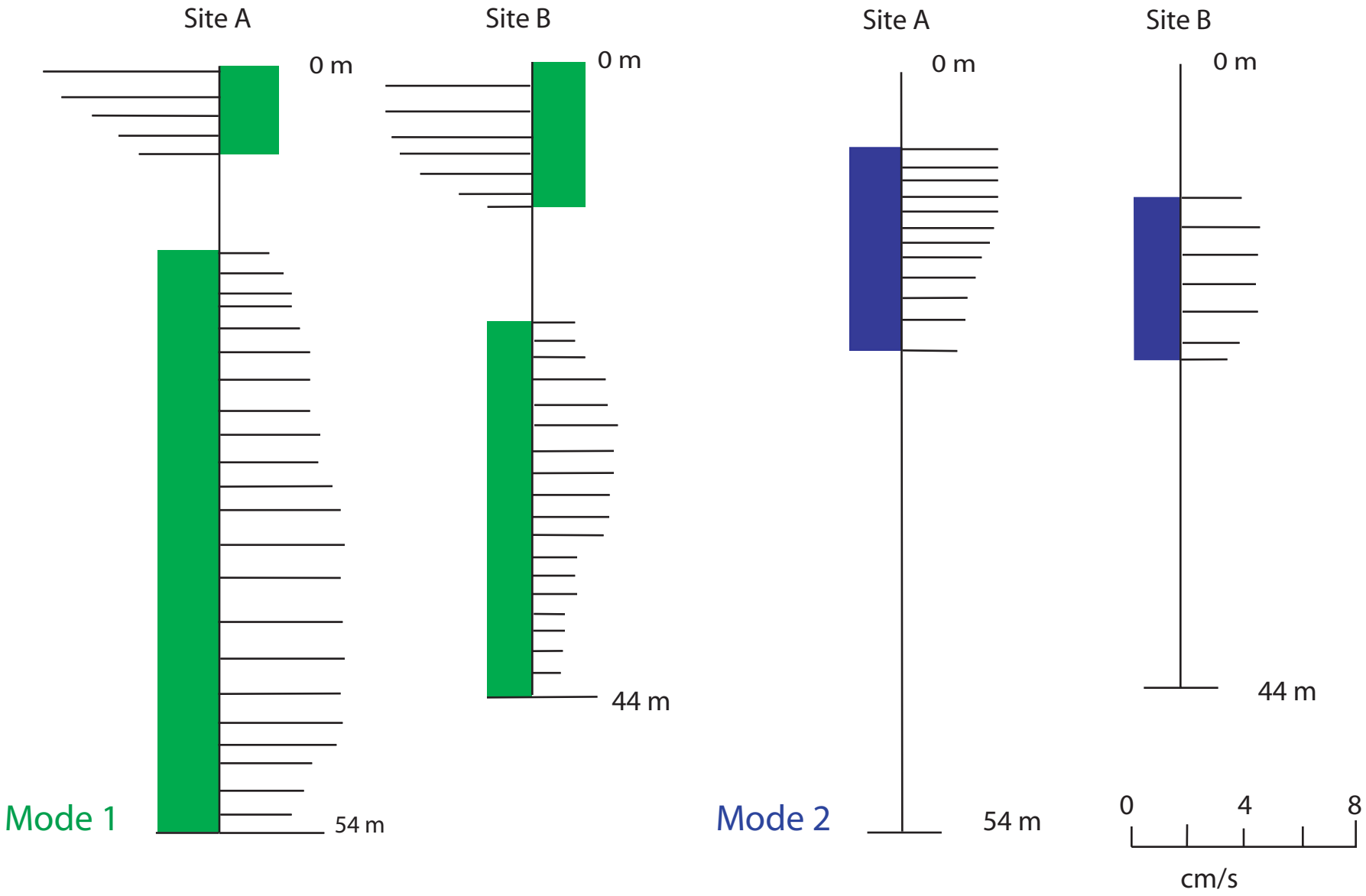

Figure 9. Vertical structure of subtidal alongcanal currents in Modes 1 and 2. The horizontal lines show the vertical shear in current velocity with depth. If currents at a particular depth are not associated with the mode, no horizontal line is plotted.

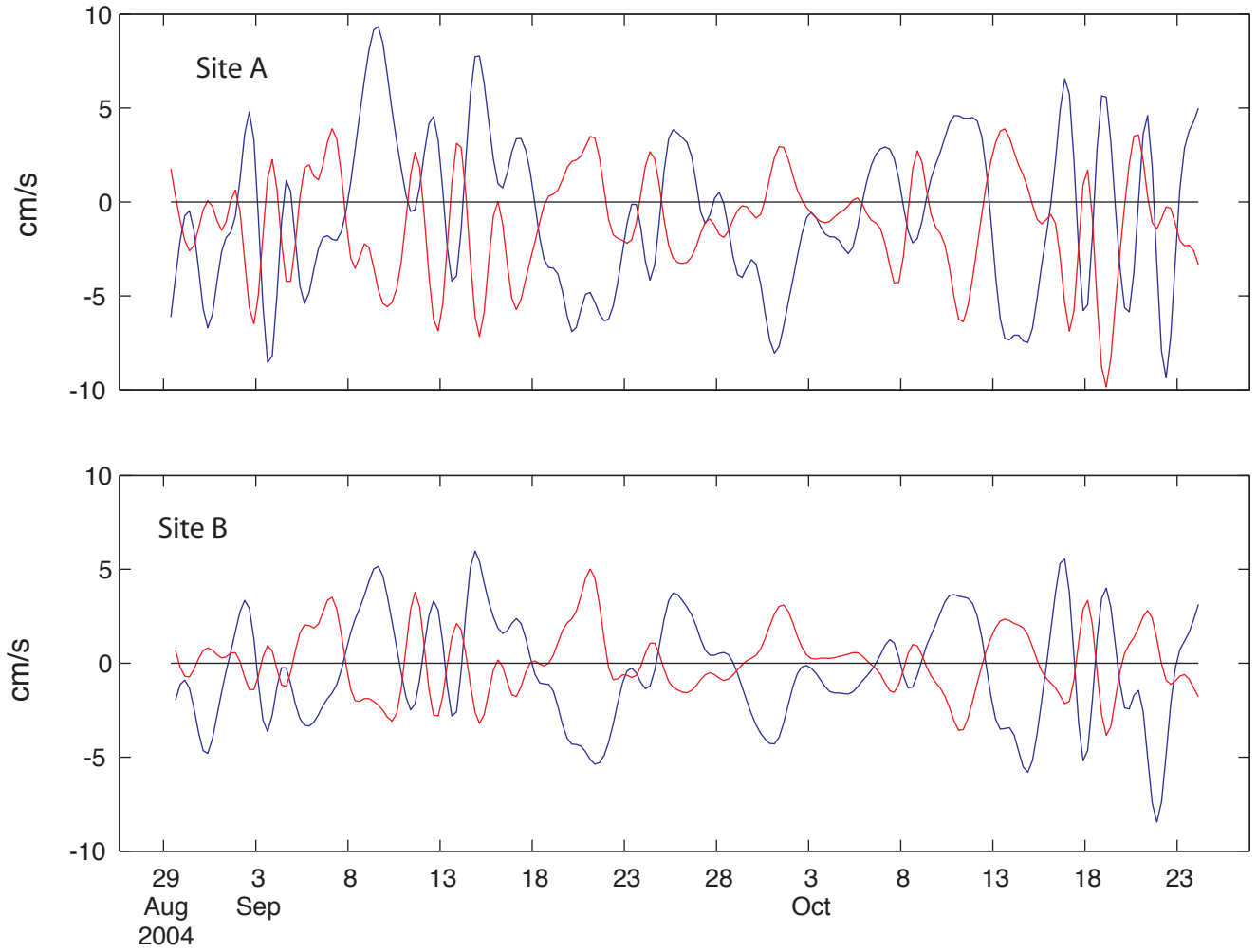

Figure 10. Subtidal currents averaged over the surface (blue) and bottom layers (red) of Mode 1 at Sites A and B.

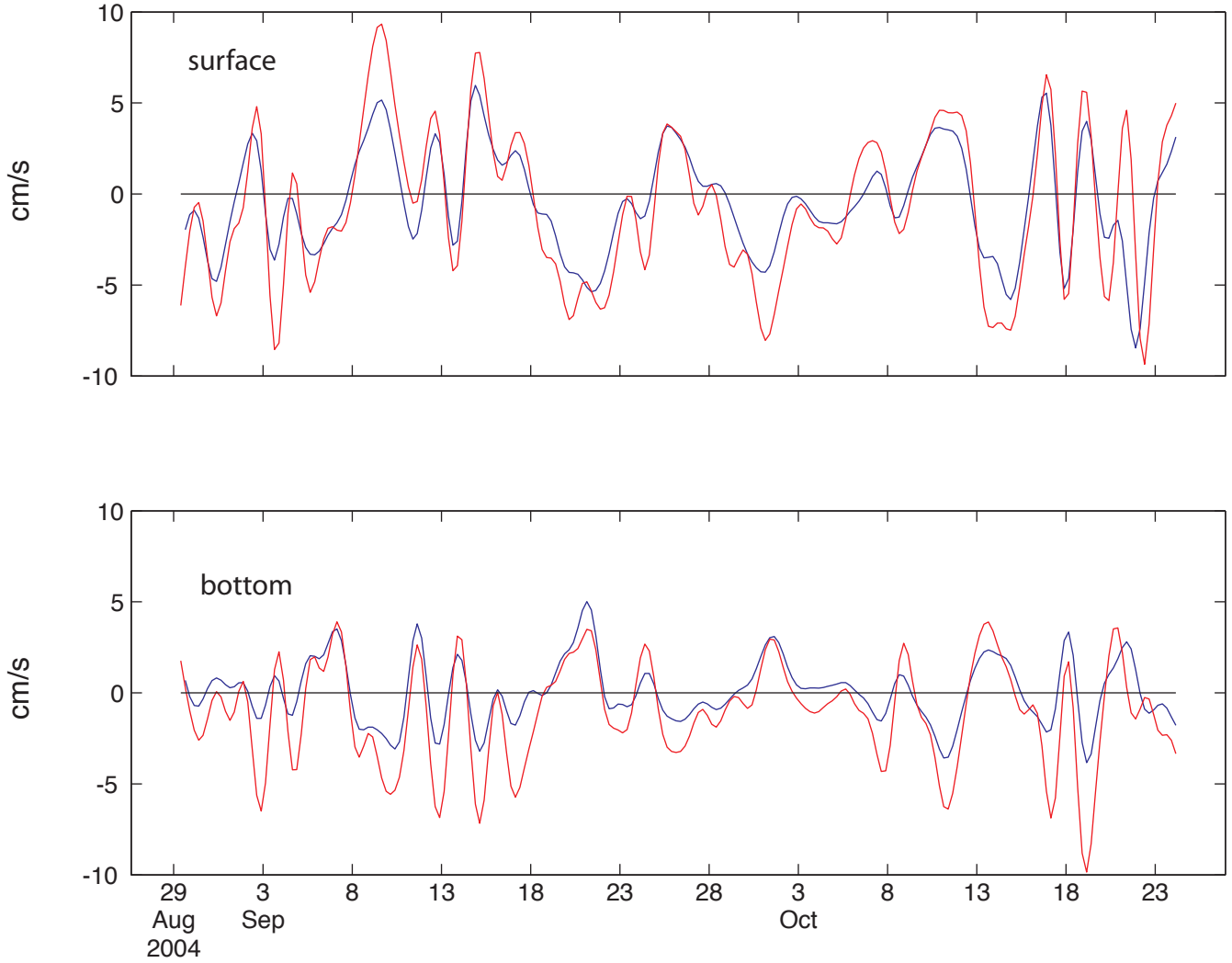

Figure 11. Subtidal currents averaged over the surface and bottom layers of Mode 1 at Site B (blue) and A (red).

occupy 50 to 100 percent of the length of Hood Canal. It is not clear what forces this internal seiche, but it is probable that the seiche is persistent. Our measurements suggest that it was present during the entire two-month deployment.

In order to determine whether winds could be partially responsible for forcing the seiche, wind measurements were obtained from Shelton, Washington, a town about 10 miles south of the canal. Given the prevalent mountains and hills around Hood Canal, the direction of winds at Shelton may not represent the wind direction over the canal, but the wind strength could be correlated between the two regions. If it is windy at Shelton, it should be windy at Hood Canal.

Winds at Shelton were converted to wind stress using a formula by Wu (1980), then low-pass filtered to produce records with fluctuations at periods similar to those found in the baroclinic seiche. Wind stress was then rotated into a component aligned with the direction of maximum wind stress amplitude using the principal axes (prominent direction) of the subtidal wind stress velocity. Positive winds aligned along the principal axes flowed toward Hood Canal and were highly correlated with winds at Shelton blowing toward the north, roughly aligned with the axis of Hood Canal.

Fluctuations in the principal-axis wind stress seem correlated with currents in the baroclinic seiche (Figure 12). At the beginning and end of the measurement program, relatively strong wind-stress fluctuations with periods of a few days were followed by similar fluctuations in current about one day later. A statistical analysis shows that 22 percent (34 percent) of the surface (lower-layer) currents at Site A (Table 5) were correlated with wind stress. The correlations were slightly weaker at Site B, where only correlations in the lower layer were significant at the 95 percent confidence level. A coherence analysis between wind stress and modal currents at Sites A and B indicates that wind stresses with periods of 2-3 days had the strongest correlations with seiche currents, consistent with the pattern shown in Figure 12. Roughly 50 percent of the current energy in these periods is associated with wind forcing.

It is interesting to note that the daily flow from the Cushman Powerhouse on the western side of the Great Bend has fluctuations with periods similar to those found in the seiche (Figure 13). For the first third of the measurement period, an increase in flow from the Powerhouse was associated with surface currents in Hood Canal flowing seaward toward the mouth of the canal. This flow pattern tended to reverse in the latter portion of the record, with surface currents flowing toward Lynch Cove when the flow from the Powerhouse increased. Given that the flow from the Powerhouse enters Hood Canal at Potlatch, in the middle of the Great Bend, it may not be surprising that, at times, surface currents bend toward the mouth (seaward) of the canal, and at other times bend toward Lynch Cove. On average, surface flows in the 3-4 day frequency band were coherent and flowing toward Lynch Cove when flow from the powerhouse increased. Only a small percentage of the total variance in surface currents was associated with flow from the Powerhouse; values were generally less than 15 percent. Wind-stress forcing appeared to be the more dominant process. However, this was a very short measurement period; the relative importance of the various forcing processes may not be robust. Clearly, many processes could contribute to the internal seiche in Hood Canal, and more measurements must be collected before these connections between the several flow patterns can be confirmed.

The second mode for subtidal currents accounted for most of the remaining subtidal current variability in Hood Canal (Table 4b; Figures 9, 14). It was present only near the thermocline, where the first mode was weakest (Figure 9) and was not coherent with the first mode. Again, currents at the two sites tended to flow in the same direction (Figure 15), though the coherence was not as strong as for mode 1. Coherence amplitude was 0.6, suggesting that only 36 percent

Table 4a. Mode 1 subtidal current statistics. Only currents significantly correlated with the mode are included in the modal structure. The zero level for the squared coherence is 0.21. Lower layer currents are assumed to reach the bed.

Site	Percentage variance	Width of surface layer	Top of lower layer	Width of lower layer
A	75	6 m	13 m	41 m
B	63	11 m	18 m	26 m

Table 4b. Mode 2 subtidal current statistics. Only currents significantly correlated with the mode are included in the modal structure. The zero level for the squared coherence is 0.21.

Site	Percentage variance	Shallowest layer for Mode 2 current	Deepest layer for Mode 2 current
A	18	4 m	18 m
B	22	9 m	21 m

Table 5. The correlation between wind stress and currents in the internal seiche in Hood Canal. The wind stress is aligned with the principal axis of wind measured at Shelton WA, a city 10 miles south of Hood Canal. A positive wind blows toward the north, toward the mouth of the canal. A positive lag means the first record leads the second. The 95% confidence for zero coherence is 0.45.

Record 1	Record 2	Correlation	Lag (Days)
Wind stress	Surf A	0.47	1
Wind stress	Bottom A	-0.58	1
Wind stress	Surf B	-	-
Wind stress	Bottom B	-0.45	1

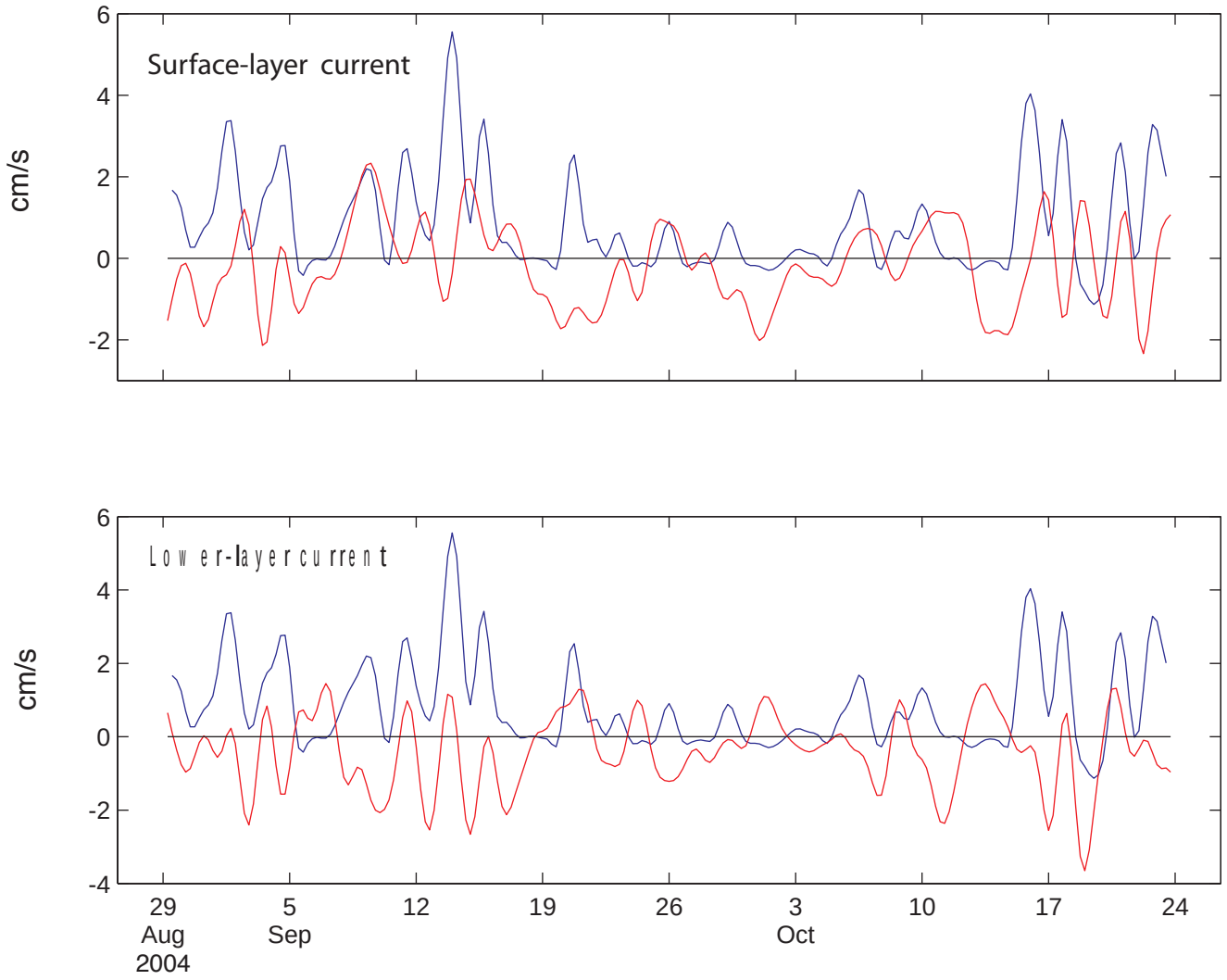

Figure 12. The principal axis of wind stress at Shelton, WA (blue), and surface and lower-layer currents in the internal seiche at site A (red). For clarity, wind-stress amplitudes have been multiplied by 100.

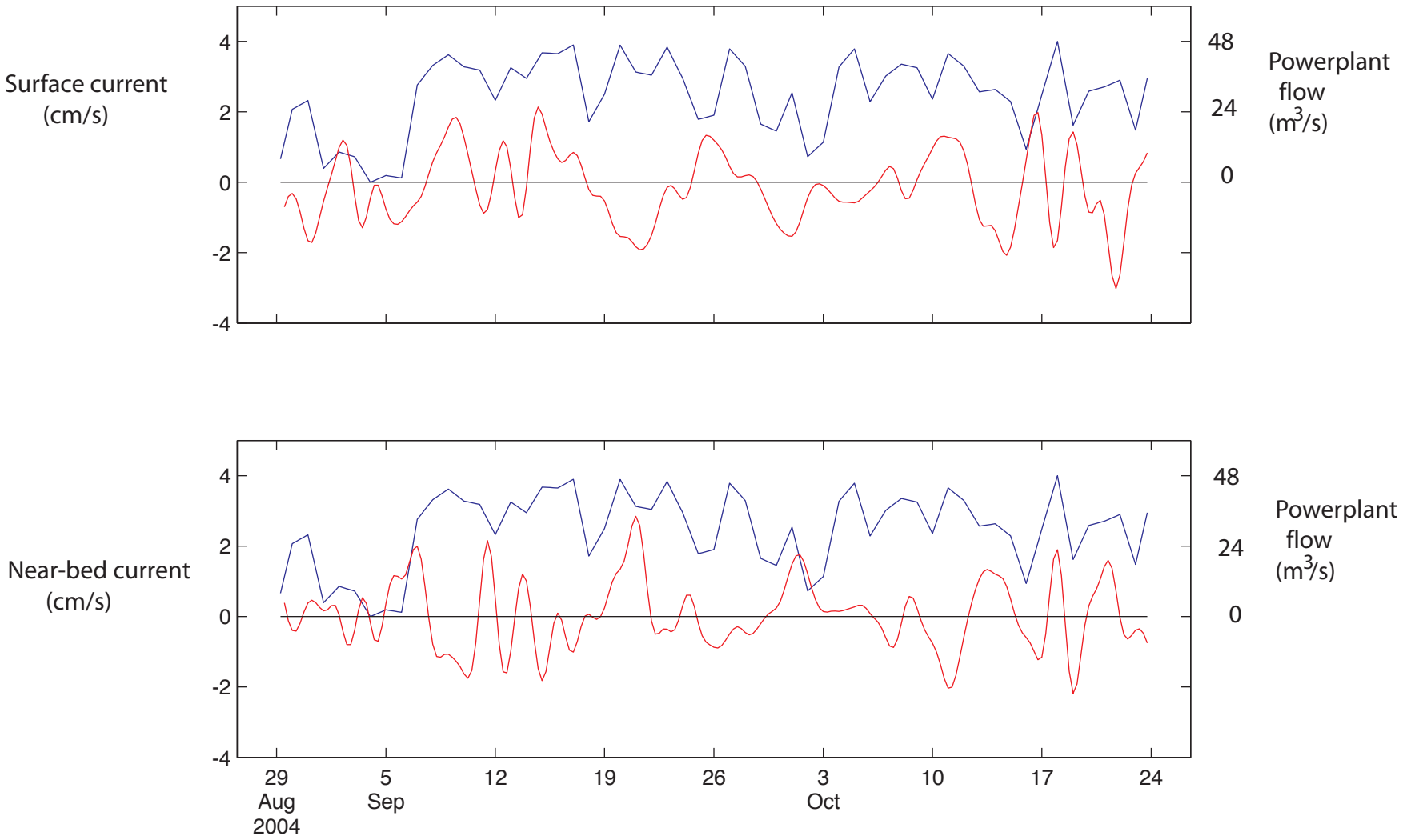

Figure 13. Subtidal currents averaged over the surface and bottom layers for Mode 1 at Site A (red) and flow into Hood Canal from the Cushman Powerplant at Potlatch (blue). For clarity, currents in the surface (bottom) layer have been divided by 2.8 (1.7).

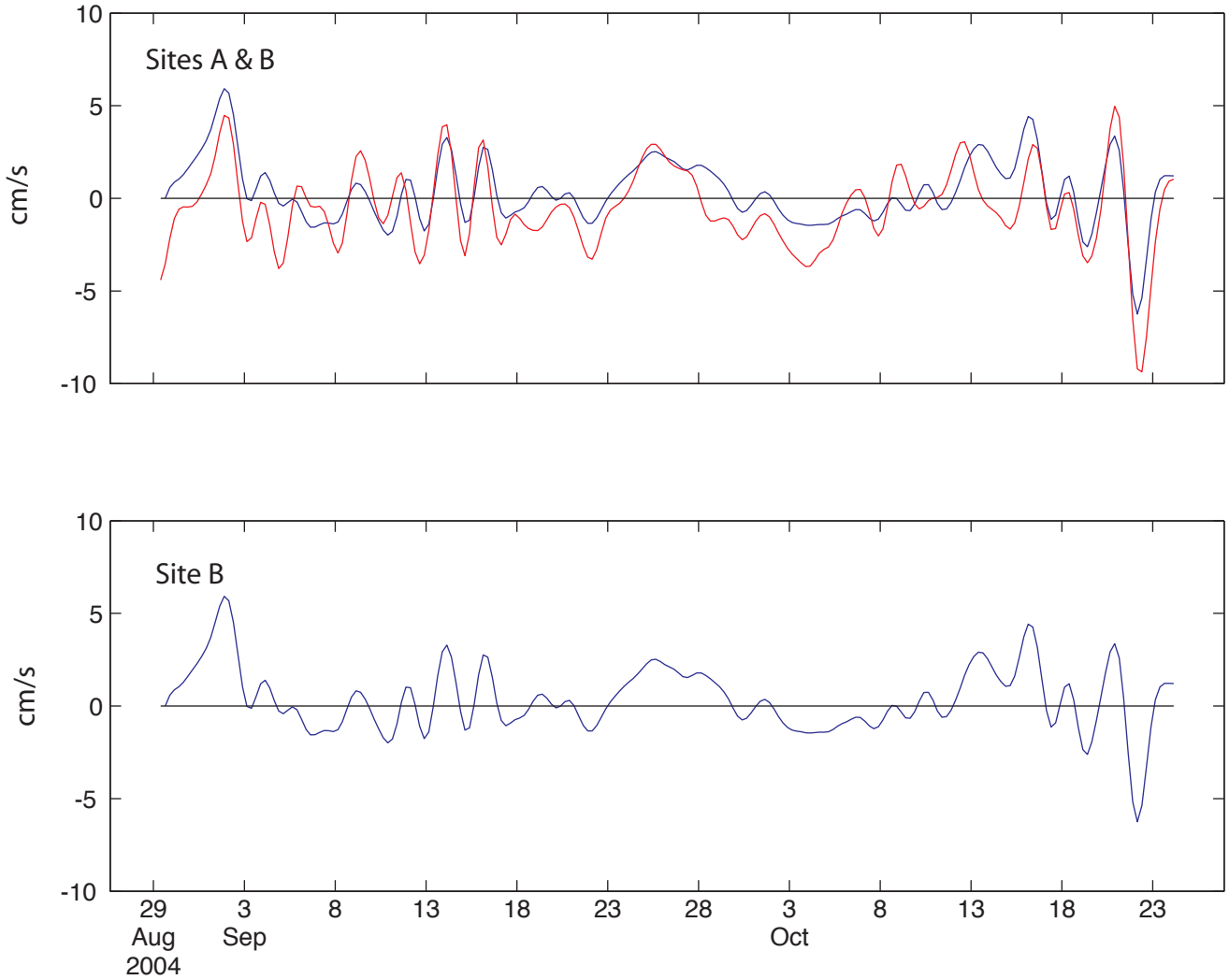

Figure 14. Vertically averaged subtidal along-canal currents of Mode 2 at Sites A (red) and B (blue).

of the energy was coherent between the two sites (Table 3). Despite the change in canal width, the amplitudes of the coherent fluctuations were similar at both sites.

WATER PROPERTY OBSERVATIONS

Subtidal fluctuation patterns

The temperature, salinity, and oxygen content of the water near the bed increased markedly about halfway through the measurement period (Figure 15). A pool of warmer, saltier, and more oxygenated water near the bed passed over Site B, then Site A in mid-September. A rough estimate of the frontal passage between the two sites suggests the warmer water traveled toward the head (landward) of the canal at about 1 cm/s, roughly at the mean current speed at Site A. The warmer, more oxygenated water remained in the region at least until the end of October, at the end of our measurement program.

CTD casts show that the changes in water properties measured near the bed by the moorings in September and October actually represent changes in the water properties from the bed to within 15-20 m of the surface (Figures 6a-d). During these periods, temperatures below 15 m varied by less than a degree and salinities varied by less than 1 PSU. The changes in the CTD profiles show that the entire portion of the water column below the thermocline was warmer, saltier, and more oxygenated in October than in September, consistent with the moored time-series measurements made near the bed. It is of interest to note that this portion of the water column occupied the same depth range, represented by the lower layer of the first subtidal current mode (Table 4a). Hence, the water column from 15 m to the bed not only had similar water properties, but it moved uniformly up and down the canal over the two-month deployment period.

This change in near-bed water properties was not associated with a similar change in the current patterns in Hood Canal. The mean and subtidal flow patterns did not show any systematic change between the first and second half of the measurement period.

Fluctuation patterns at tidal frequencies

The tidal currents are the largest current component in Hood Canal. A close examination of the relationship between tidal current flow and frontal passage confirms that the warmer, saltier, and more oxygenated water was moving slowly toward Lynch Cove, at the landward end of Hood Canal. When tidal currents flowed seaward toward the mouth of the canal in mid-September, the water at each site became fresher, cooler, and less oxygenated (Figure 16). The amplitude of the fluctuations in water properties at Site B was stronger than at Site A, despite the fact that the tidal excursions at Site B were weaker than at Site A. This suggests that the front in water properties became more diffuse as it moved up the canal. It may have mixed with the surrounding water as it was being advected toward Lynch Cove.

The phases in the diurnal and semidiurnal tidal bands between currents and water properties support the advection of a front toward the Lynch Cove end of the canal (Tables 6, 7). The near-90-degree phase shift and the fact that water properties lead the currents suggest that warmer, saltier, and more oxygenated water tends to be found toward the mouth (seaward) of Hood Canal for the entire measurement period. At Site B, most of the tidal-band fluctuations in higher oxygen were associated with warmer, saltier water (Tables 6, 7). Coherence levels were above

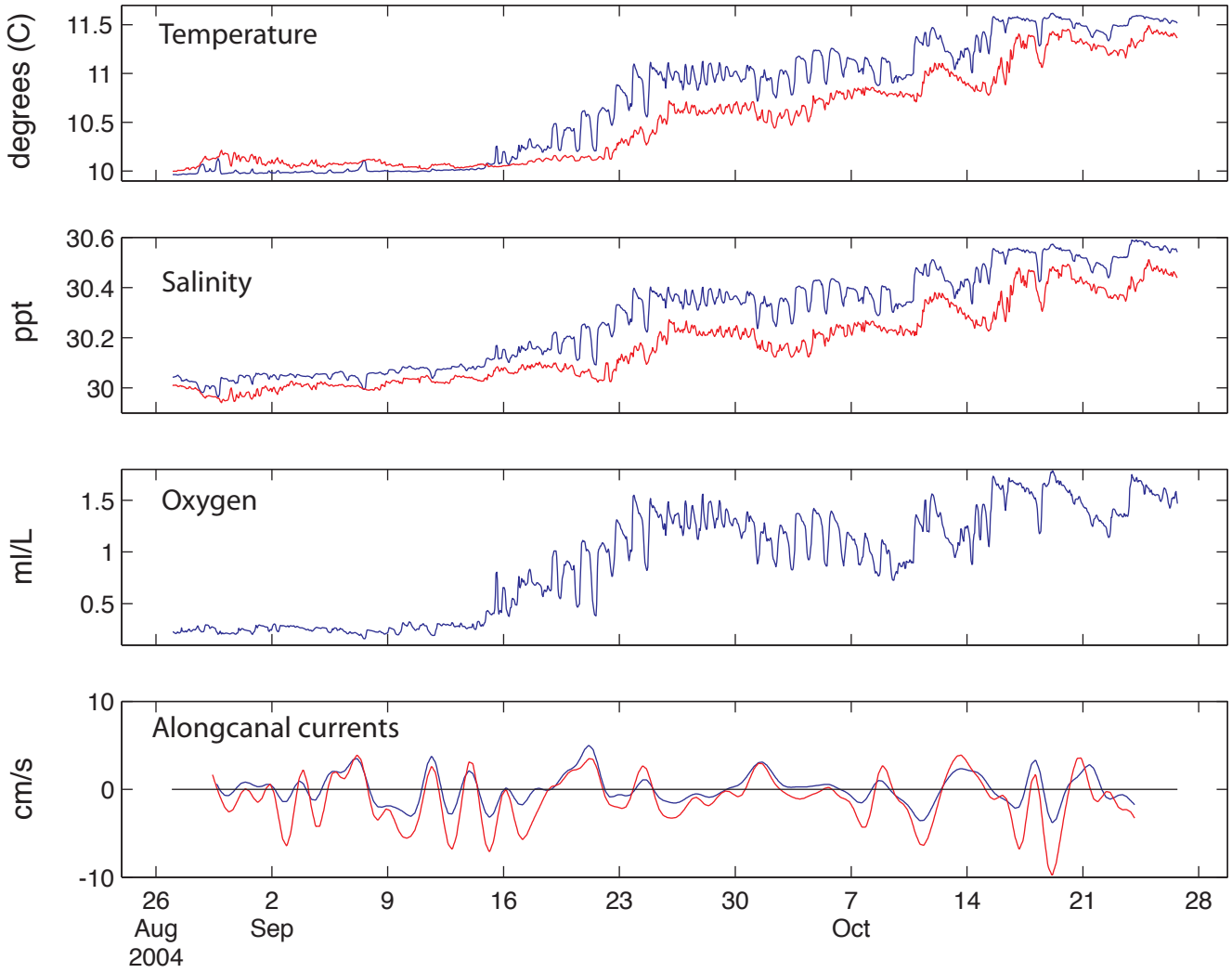

Figure 15. Subtidal along-canal currents, hourly recorded oxygen, salinity, and temperature near the bed at Site A (red) and Site B (blue).

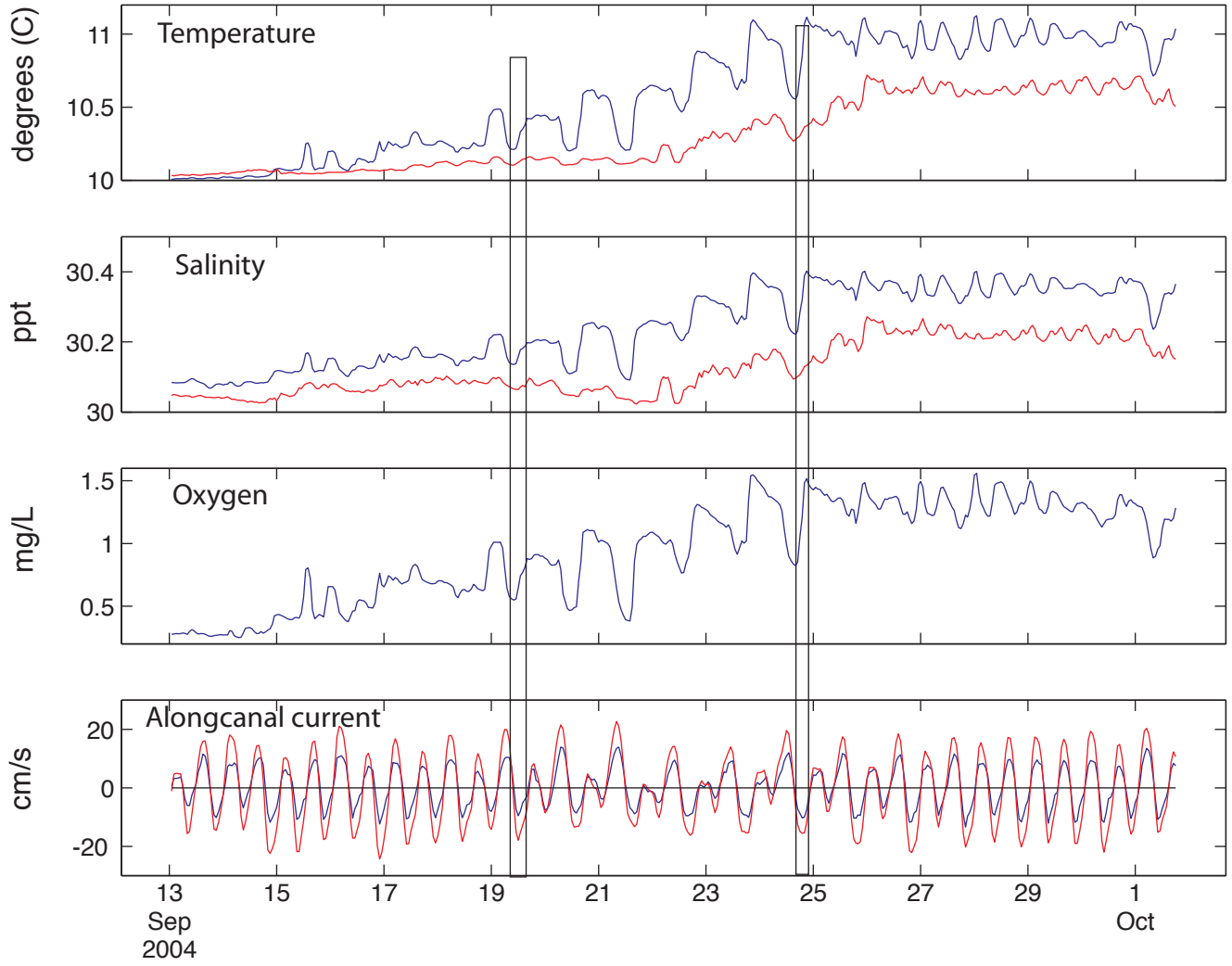

Figure 16. Tidal currents advect warmer, saltier, more oxygenated water from Site B (blue) toward Site A (red).

Table 6. Coherence among the vertically averaged current and other water properties in the diurnal tidal band. A positive phase indicates the second member of the pair led the first. The longest resolvable period is 192 hours. The coherence calculation used a hanning window with a 50 percent overlap.

Site	Site	Coherence	Phase
A_current	A_Temp	0.66	69 ± 27
	A_Salt	0.82	56 ±16
ATEMP	A_Salinity	0.92	0
B_current	B_Temp	0.69	101 ±25
	B_Salt	0.83	98 ±16
	B_Oxygen	0.78	103 ±19
B_Temp	B_Salt	0.96	0
	B_Oxygen	0.98	0
B_Salt	B_Oxygen	0.99	5 ±3
Current_B	Curr_A	0.99	5 ±3
Temp_B	Temp_A	0.64	-32 ±29
Salt_B	Salt_A	0.72	-39 ±23

Table 7. Coherence among the vertically averaged current and other water properties in the semidiurnal diurnal tidal band. A positive phase indicates the second member of the pair led the first. The longest resolvable period is 186 hours. The coherence calculation used a hanning window with a 50 percent overlap.

Site	Site	Coherence	Phase
A current	A_Temp	0.58	88 ±34
	A_salt	0.81	83 ±17
A temp	A_salt	0.87	0
B_current	B_Temp	0.71	86 ±23
	B_Salt	0.87	86 ±14
	B_Oxygen	0.83	83 ±16
B_Temp	B_salt	0.95	0
B_Temp	B_oxygen	0.98	0
B_Salt	B_Oxygen	0.99	0
Curr_b	Curr_A	1.0	4
Temp_B	Temp_A	0.82	0
Salt_B	Salt_A	0.83	0

0.95. Tidal current amplitudes suggest that water-property fronts are moved back and forth at 1-3 km per day. Given that the fluctuations in temperature and salinity were highly coherent between sites that are 5 km apart, this suggests that fronts in water properties have length scales at least that large.

CONCLUSIONS

Measurements collected in the fall of 2004 at two locations near the head of Hood Canal show that tidal currents are the dominant current component in the canal. The tidal currents are aligned primarily along the axis of the canal, with the semidiurnal M_2 tidal current the largest; current amplitudes are 8 to 14 cm/s. Site A, which is located in a relatively narrow portion of the canal, has the strongest tidal currents. The increase in amplitude is roughly proportional to the decrease in cross-sectional area between Sites B and A.

The subtidal currents also flow primarily up and down the canal. The mean flow is weak, or nonexistent, in the canal except in the seabed at Site A. Here, currents flow toward the head of the canal with speeds usually less than 2.3 cm/s.

An internal seiche dominates the fluctuating portion of the subtidal flow field in Hood Canal. Subtidal currents above the shallow thermocline flow primarily along the canal, but in a direction opposite to the subtidal currents beneath the thermocline. The amplitudes of the current fluctuations are generally less than 8 cm/s, and the phase between the upper and lower layer currents is about 180°. The high correlations and small phase lags in the subtidal currents between sites suggest that this subtidal seiche has a length scale much longer than the 5-km separation between the two measurement sites. It is probable that at least a portion of the energy in the seiche is driven by the local winds that blow up and down the canal.

During the measurement program, a pool of warmer, saltier, and more oxygenated water moved past the measurement sites. A rough estimate of the speed of the frontal passage suggested this water moved toward the head of the canal with a speed of 1 cm/s. This speed is consistent with that of the mean currents measured near the bed at Site A. CTD measurements taken near the two measurement sites during the deployment indicate that this more oxygenated layer of water extended from the bed to the thermocline. Oxygen data from the tripods showed that this water remained in the region until at least the end of October 2004, when the tripods were recovered.

The spatial and temporal patterns seen in the data collected in this program are interesting, but are clearly limited. The tidal current amplitudes measured in the canal probably represent tidal current amplitudes in this region over the year. However, the data sets are too short and cover too limited a region to allow one to infer that the patterns seen in the subtidal and mean flows are either persistent or represent a large region of the canal. More data taken at different sites and over much longer time periods is needed before one can characterize the transport patterns in Hood Canal.

Data files used for this report can be obtained from Anne L. Gartner (agartner@usgs.gov), Marlene Noble (mnoble@usgs.gov), or the Coastal and Marine Geology Team Chief Scientist, U.S. Geological Survey, 345 Middlefield Road, MS 999, Menlo Park, California 94025.

REFERENCES

Collias, C.E., McGary, N., and Barnes, C.A., 1974. Atlas of physical and chemical properties of Puget Sound and its approaches. University of Washington Sea Grant Publication WSG 74-1, 285 p.

Foreman, M.G.G., 1977. Manual for tidal heights analysis and prediction. Pacific Marine Science, Institute of Ocean Sciences, Patricia Bay, Sydney, B.C., Report 77-10, 97 p.

— 1978. Manual for tidal currents analysis and prediction. Pacific Marine Science, Institute of Ocean Sciences, Patricia Bay, Sydney, B.C., Report 78-6, 70 p.

Godin, G., 1972. The analysis of tides. University of Toronto Press, Toronto, 264 p.

Joreskog, K.G., Klovan, J.E., and Reyment, R.A., 1976. Geological factor analysis. Elsevier, New York, 178 p.

Lipscomb, S.W., 1995. Quality assurance plan for discharge measurements using broad band acoustic Doppler current profilers. U.S. Geological Survey Open-File Report 95-701, 7 p.

Norris, J.M., 2001. Policy and technical guidance on discharge measurements using acoustic Doppler current profilers. Office of Surface Water Technical Memorandum No. 2002.02, 4 p.

Pond, S., and Pickard, G.L., 1983. Introduction to dynamical oceanography, 2nd edition. Butterworth-Heinemann, Oxford, 329 p.

R.D. Instruments, Inc., 1996. Principals of operation. A practical primer for broad-band acoustic Doppler current profilers (2nd ed.). R.D. Instruments, Inc., San Diego, CA, 51 p.

Simpson, M.R., 2001. Discharge measurements using a broad-band acoustic Doppler current profiler. U.S. Geological Survey Open-File Report 01-1, 123 p.

Wu, J., 1980. Wind-stress coefficients over the sea surface near neutral conditions. Journal of Physical Oceanography, 10, 727-740.

Appendix A: Mean and Tidal Current Statistics

Table A-1a. Statistics for the hour-averaged current readings at Site A. The standard deviation of the subtidal current field is used to compute the error bars around the mean flow. Studies were carried out from August to October 2004; table includes statistics for whole record. Means in bold type are significantly different from zero at the 95% confidence level. Depths are calculated using pressure sensors on the Microcat instruments.

	Alongcanal (cm/s)					Crosscanal (cm/s)				
Instrument Depth (m)	Mean	Error Bar	Standard Deviation	Max	Min	Mean	Error Bar	Standard Deviation	Max	Min
3.3	-0.7	2.2	13.0	31.7	-36. 4	-0.1	0.3	2.6	14.9	-15.0
4.3	-0.7	2.0	13.0	31.7	-42.7	-0.2	0.3	2.3	13.9	-9.3
5.3	-0.9	1.7	12.5	28.3	-36.4	-0.1	0.2	2.2	7.6	-9.9
6.3	-0.9	1.5	12.2	28.1	-32.8	-0.0	0.2	2.1	7.7	-9.2
7.3	-0.8	1.4	11.9	27.9	-30.4	0.1	0.2	1.9	7.7	-7.5
8.3	-0.7	1.3	11.8	27.0	-29.0	0.2	0.2	1.9	7.1	-7.4
9.3	-0.6	1.2	11.7	27.0	-29.1	0.2	0.2	1.8	7.3	-8.0
10.3	-0.5	1.1	11.6	28.7	-27.6	0.2	0.2	1.8	7.1	-9.0
11.3	-0.4	1.1	11.6	30.7	-26.8	**0.3**	0.2	1.8	6.1	-7.9
12.3	-0.3	1.0	11.5	32.6	-26.0	**0.3**	0.2	1.7	6.6	-7.0
13.3	-0.3	1.1	11.6	33.5	-26.3	**0.3**	0.2	1.7	6.3	-7.1
14.3	-0.2	1.1	11.6	33.4	-28.3	**0.3**	0.2	1.6	6.3	-6.4
15.3	-0.2	1.1	11.6	33.8	-29.6	**0.3**	0.2	1.6	5.9	-5.9
16.3	-0.1	1.1	11.7	34.1	-28.9	**0.4**	0.2	1.6	5.6	-4.9
17.3	-0.1	1.2	11.7	34.0	-28.9	**0.4**	0.2	1.6	5.7	-4.9
18.3	-0.1	1.2	11.8	34.1	-28.9	**0.4**	0.2	1.5	5.3	-5.5
19.3	-0.1	1.2	11.8	35.0	-29.0	**0.4**	0.2	1.5	5.4	-5.6
20.3	-0.1	1.2	11.9	34.9	-28.7	**0.4**	0.1	1.5	5.0	-5.2
21.3	-0. 2	1.2	11.9	35.5	-28.5	**0.4**	0.1	1.5	5.0	-4.7
22.3	-0.2	1.2	12.0	35.2	-28.4	**0.4**	0.1	1.4	4.8	-4.5
23.3	-0.2	1.3	12.1	34.9	-28.9	**0.4**	0.1	1.4	4.6	-4.7
24.3	-0.3	1.3	12.2	34.5	-28.9	**0.4**	0.1	1.4	4.7	-5.0
25.3	-0.4	1.32	12.2	34.3	-29.5	**0.4**	0.1	1.4	4.5	-4.9

Table A-1a, cont.

	Alongcanal (cm/s)					Crosscanal (cm/s)				
Instrument Depth (m)	Mean	Error Bar	Standard Deviation	Max	Min	Mean	Error Bar	Standard Deviation	Max	Min
26.3	-0.5	1.3	12.3	33.8	-29.6	**0.4**	0.1	1.3	4.8	-4.9
27.3	-0.6	1.3	12.3	33.6	-29.7	**0.4**	0.1	1.3	5.0	-4.6
28.3	-0.7	1.3	12.3	33.5	-30.2	**0.3**	0.1	1.3	5.7	-3.8
29.3	-0.9	1.4	12. 4	33.5	-30.7	**0.3**	0.1	1.2	5.9	-3.8
30.3	-1.0	1.4	12.4	33.7	-31.5	**0.3**	0.1	1.2	5.2	-4.3
31.3	-1.1	1.4	12.5	33.5	-31.0	**0.3**	0.1	1.2	5.3	-4.6
32.3	-1.2	1.4	12.5	33.3	-31.5	**0.3**	0.1	1.2	5.4	-4.4
33.3	-1.4	1.4	12.5	33.0	-31.1	**0.2**	0.1	1.2	5.1	-3. 9
34.3	**-1.5**	1.4	12.6	32.1	-31.1	**0.2**	0.1	1.2	4.4	-3.8
35.3	**-1.6**	1.4	12.6	31.9	-31.3	**0.2**	0.1	1.2	4.8	-3.7
36.3	**-1.7**	1.4	12.6	31.9	-31.6	**0.2**	0.1	1.1	4.6	-3.6
37.3	**-1.8**	1.4	12.6	32.1	-32.0	**0.2**	0.1	1.1	4.8	-4.0
38.3	**-1.9**	1.4	12.7	31.9	-32. 2	**0.2**	0.1	1.1	4.9	-3.8
39.3	**-1.9**	1.4	12.7	31.7	-33.0	**0.2**	0.1	1.1	4.8	-4.1
40.3	**-2.0**	1.4	12.7	31.6	-32.5	**0.2**	0.1	1.2	5.6	-3.8
41.3	**-2.1**	1.4	12.6	31.5	-32.4	**0.2**	0.1	1.2	5.5	-4.1
42.3	**-2.1**	1.4	12.6	31.9	-32.9	**0.2**	0.1	1.3	5.9	-4.9
43.3	**-2.2**	1.4	12.5	31.0	-32. 6	**0.2**	0.1	1.4	6.4	-4.8
44.3	**-2.2**	1.4	12.4	31.1	-31. 9	**0.2**	0.1	1.5	6.7	-5.6
45.3	**-2.2**	1.4	12.3	30.2	-32.3	**0.2**	0.1	1.6	7.3	-5.4
46.3	**-2.3**	1.3	12.1	29.5	-32.4	**0.3**	0.2	1.8	8.1	-5.7
47.3	**-2.3**	1.3	11.8	29.0	-32.0	**0.4**	0.2	1.9	8. 2	-5.5

Table A-1b. Statistics for the hour-averaged currents at Site B. The standard deviation of the subtidal current field is used to compute the error bars around the mean flow. Studies were carried out from August to October 2004; table includes statistics for whole record. Means in bold type are significantly different from zero at the 95% confidence level. Depths are calculated using pressure sensors on the Microcat instruments.

	Alongcanal (cm/s)					Crosscanal (cm/s)				
Instrument Depth (m)	Mean	Error Bar	Standard Deviation	Max	Min	Mean	Error Bar	Standard Deviation	Max	Min
3.9	0.2	1.9	9.1	30.8	-40.7	0.5	0.5	3.4	33.2	-22.7
4.9	-0.1	1.8	9.2	40.6	-26. 6	0.5	0.5	3.2	10.8	-23.4
5.9	-0.6	1.6	8.7	38.1	-27.2	**0.6**	0.4	2.9	13.2	-9.2
6.9	-0.8	1.4	8.3	31.4	-26.5	**0.6**	0.4	2.8	10.5	-8.2
7.9	-0.8	1.3	8.0	26.0	-25.3	**0.5**	0.4	2.7	9.3	-8.6
8.9	-0.7	1.2	7.7	19.5	-26.6	0.4	0.5	2.7	9.3	-8.3
9.9	-0.5	1.1	7.3	19.8	-26.9	0.3	0.4	2.6	8.8	-8.3
10.9	-0.3	1.0	7.0	20.3	-25.9	0.3	0.3	2.5	8.1	-8.8
11.9	-0.0	1.0	6.8	20.3	-23.8	0.2	0.3	2.4	7.3	-8.8
12.9	0.2	0.9	6.7	20.9	-21.9	0. 3	0.3	2.4	9.3	-7.6
13.9	0.4	0.9	6.6	22.1	-19.8	0.2	0.3	2.2	9.6	-7.2
14.9	0.6	0.9	6.6	24.9	-19.2	0.2	0.2	2.1	9.9	-6.8
15.9	0.7	0.9	6.6	26.7	-17.7	0.2	0.2	1.9	9.9	-6.6
16.9	0. 8	0.9	6.7	28.7	-15.8	0.2	0.2	1.8	10.2	-7.0
17.9	0.8	0.9	6.8	29.6	-14.7	0.1	0.3	1.8	9.3	-5.7
18.9	0.9	0.9	6.9	29.2	-14.2	0.2	0.2	1.8	10.1	-4.7
19.9	0.8	1.0	7.0	28.8	-14.7	0.2	0.3	1.8	10.4	-6.1
20.9	0.8	1.0	7.1	28.5	-15.3	0.2	0.3	1.8	10.5	-5.8
21.9	0.7	1.0	7.2	29.3	-16.1	0.3	0.3	1.8	9.8	-5.6
22.9	0.5	1.0	7.3	28.6	-15.9	0.2	0.3	1.9	9.5	-6.0
23.9	0.3	1.0	7.3	28. 3	-15.5	0.2	0.3	1.9	9.6	-6.1
24.9	0.2	1.1	7.4	28.3	-17.1	0.2	0.3	1.9	9.3	-5.7
25.9	0.0	1.1	7.4	28.0	-17.1	0.1	0.3	2.0	8.8	-5.6

Table A-1b, cont.

	Alongcanal (cm/s)					Crosscanal (cm/s)				
Instrument Depth (m)	Mean	Error Bar	Standard Deviation	Max	Min	Mean	Error Bar	Standard Deviation	Max	Min
26.9	-0.1	1.1	7.4	27.5	-17.2	0.1	0.3	2.0	7.8	-6.2
27.9	-0.2	1.0	7.4	27.0	-17.9	0.1	0.3	2.1	6.8	-5.6
28.9	-0.3	1.0	7.3	26.8	-17.8	0.1	0.3	2.1	6.7	-5.9
29.9	-0.4	1.0	7.3	27.4	-18.5	0.0	0.3	2.1	6.5	-6.1
30.9	-0.4	1.0	7.2	27.0	-18.0	0.0	0.3	2.1	6.2	-7.4
31.9	-0.4	0.9	7.1	25.8	-18.9	-0.0	0.3	2.0	5.8	-7.6
32.9	-0.4	0.8	6.9	23.8	-18.0	-0.1	0.3	2.0	6.1	-8.5
33.9	-0.4	0.8	6.8	23.3	-17.3	-0.1	0.3	1.9	5.2	-7.8
34.9	-0.3	0.7	6.6	21.4	-16.9	-0.2	0.3	1.8	4.9	-8.0
35.9	-0.2	0. 7	6.5	20.4	-16.5	-0.2	0.3	1.7	5.1	-7.3
36.9	-0.1	0.6	6.2	19.4	-16.5	-0.2	0.3	1.6	4.6	-6.9
37.9	0.0	0.6	6.0	17.8	-15.5	-0.3	0.3	1.6	4.7	-6.5

Table A-2. Barotropic tides, summed over 45 bins for Site A and over 35 bins for Site B. Studies were carried out from August to October 2004; table includes statistics for whole record. A 90-degree inclination indicates the major axis of the tide is aligned parallel to the local axis of the canal. Sea-level fluctuations are measured by a pressure sensor. A 1-decibar pressure measurement represents a 1-m change in sea level. A positive minor axis indicates the tidal currents rotate anticlockwise. Depths are calculated using pressure sensors on the Microcat instruments.

Site A						
	Current				Pressure	
	Major axis (cm/s)	Minor axis (cm/s)	Inclination (degrees)	Phase (degrees)	Amplitude (dbar/s)	Phase (degrees)
Tide						
O_1	3.1	-0.1	90	349	0.5	239
K_1	5.0	-0.1	90	3	0.6	259
M_2	13.7	0.1	91	86	1.1	337
S_2	4.7	0.0	90	108	0.4	358

Site B						
	Current				Pressure	
	Major axis (cm/s)	Minor axis (cm/s)	Inclination (degrees)	Phase (degrees)	Amplitude (dbar/s)	Phase (degrees)
Tide						
O_1	1.6	-0.3	92	360	0.5	238
K_1	2.6	-0.3	91	16	0.6	259
M_2	7.8	-0.5	95	104	1. 1	337
S_2	2.6	-0.2	99	127	0.4	358

Table A-3a. Characteristics of diurnal O_1 tidal currents with depth at Site A. Current characteristics were calculated between August and October 2004. A 90-degree inclination is the major axis of the tide aligned parallel to the local axis of the canal. Phase is defined so that the major axis of the tidal ellipse has a positive crosscanal component. A positive minor axis indicates the tidal currents rotate anticlockwise. Depths are calculated using pressure sensors on the Microcat instruments.

Depth (m)	Major Amplitude (cm/s)	Minor Amplitude (cm/s)	Inclination (degrees)	Phase (degrees)
3.3	4.5	-0.3	90	322
4.3	4.9	-0.1	88	331
5.3	4.7	-0.0	89	336
6.3	4.5	0.0	90	342
7.3	4.3	-0.0	90	347
8.3	4.2	-0.0	90	349
9.3	4.1	-0.0	90	351
10.3	4.0	0.0	90	352
11.3	3.9	0.0	90	353
12.3	3.8	-0.0	89	354
13.3	3.7	-0.0	90	355
14.3	3.6	-0.0	90	355
15.3	3.6	-0.0	91	356
16.3	3.4	-0.0	91	356
17.3	3.3	-0.1	92	356
18.3	3.3	-0.0	92	357
19.3	3.2	-0.0	93	356
20.3	3.1	0.0	92	356
21.3	3.1	0.0	92	356
22.3	3.0	0.1	91	355
23.3	2.9	0.1	91	354
24.3	2.9	0.1	90	353
25.3	2.8	0.0	91	352
26.3	2.8	0.0	90	352
27.3	2.8	0.0	90	352
28.3	2.7	0.0	90	351
29.3	2.7	-0.0	89	352
30.3	2.7	-0.0	90	352
31.3	2.7	-0.0	90	352
32.3	2.7	-0.1	90	352
33.3	2.7	-0.1	90	351
34.3	2.7	-0.1	90	350
35.3	2.6	-0.1	90	349
36.3	2.6	-0.1	90	349

Table A-3a, cont.

Depth (m)	Major Amplitude (cm/s)	Minor Amplitude (cm/s)	Inclination (degrees)	Phase (degrees)
37.3	2.6	-0.1	90	348
38.3	2.6	-0.1	90	348
39.3	2.5	-0.1	91	347
40.3	2.5	-0.2	91	346
41.3	2.4	-0.2	91	345
42.3	2.4	-0.2	92	344
43.3	2.3	-0.2	93	343
44.3	2.3	-0.2	93	342
45.3	2.2	-0.2	94	341
46.3	2.1	-0.2	95	340
47.3	2.1	-0.2	95	339

Table A-3b. Characteristics of diurnal K_1 tidal currents with depth at Site A. Current characteristics were calculated between August and October 2004. A 90-degree inclination is the major axis of the tide aligned parallel to the local axis of the canal. Phase is defined so that the major axis of the tidal ellipse has a positive crosscanal component. A positive minor axis indicates the tidal currents rotate anticlockwise. Depths are calculated using pressure sensors on the Microcat instruments.

Depth (m)	Major Amplitude (cm/s)	Minor Amplitude (cm/s)	Inclination (degrees)	Phase (degrees)
3.3	4.7	-0.2	87	3
4.3	5.0	0.1	88	7
5.3	5.0	0.1	89	10
6.3	5.2	0.1	90	11
7.3	5.3	-0.0	90	11
8.3	5.3	-0.0	90	11
9.3	5.2	0.0	90	11
10.3	5.2	0.1	90	10
11.3	5.1	-0.0	90	10
12.3	5.1	-0.1	90	10
13.3	5.0	-0.1	90	9
14.3	5.0	-0.1	90	9
15.3	5.0	-0.1	91	9
16.3	5.0	-0.2	91	9
17.3	5.0	-0.2	91	8
18.3	5.0	-0.1	91	7
19.3	5.0	-0.1	91	7
20.3	5.0	-0.1	91	6
21.3	5.0	-0.1	90	6
22.3	5.0	-0.1	90	5
23.3	5.0	-0.0	90	4
24.3	5.1	-0.0	90	4
25.3	5.1	-0.0	89	3
26.3	5.1	-0.0	89	3
27.3	5.1	-0.0	89	2
28.3	5.1	-0.0	89	2
29.3	5.1	-0.0	89	1
30.3	5.1	-0.0	89	1
31.3	5.1	-0.0	89	1
32.3	5.1	-0.06	88	1
33.3	5.2	-0.0	88	0
34.3	5.1	-0.1	88	360
35.3	5.1	-0.1	88	359
36.3	5.1	-0.1	88	359

Table A-3b, cont.

Depth (m)	Major Amplitude (cm/s)	Minor Amplitude (cm/s)	Inclination (degrees)	Phase (degrees)
38.3	5.1	-0.1	89	358
39.3	5.0	-0.1	89	358
40.3	5.0	-0.1	90	357
41.3	5.0	-0.1	90	356
42.3	4.9	-0.1	91	356
43.3	4.9	-0.1	92	356
44.3	4.8	-0.2	92	355
45.3	4.7	-0.2	93	355
46.3	4.7	-0.1	94	355
47.3	4.5	-0.2	95	354

Table A-3c. Characteristics of semidiurnal M_2 tidal currents with depth at Site A. Current characteristics were calculated between August and October 2004. A 90-degree inclination is the major axis of the tide aligned parallel to the local axis of the canal. Phase is defined so that the major axis of the tidal ellipse has a positive crosscanal component. A positive minor axis indicates the tidal currents rotate anticlockwise. Depths are calculated using pressure sensors on the Microcat instruments.

Depth (m)	Major Amplitude (cm/s)	Minor Amplitude (cm/s)	Inclination (degrees)	Phase (degrees)
3.3	12.6	-0.9	87	88
4.3	13.4	-0.5	88	89
5.3	13.3	-0.3	89	89
6.3	13.2	-0.1	90	90
7.3	13.1	-0.0	91	90
8.3	13.0	0.1	91	90
9.3	12.9	0.2	91	90
10.3	12.9	0.3	92	90
11.3	12.9	0.3	92	90
12.3	12.9	0.3	92	89
13.3	12.9	0.3	92	89
14.3	13.0	0.3	92	88
15.3	13.0	0.3	92	88
16.3	13.0	0.3	92	88
17.3	13.1	0.4	92	87
18.3	13.1	0.4	91	87
19.3	13.2	0.4	91	87
20.3	13.2	0.4	91	86
21.3	13.3	0.4	90	86
22.3	13.5	0.4	90	86
23.3	13.6	0.3	89	86
24.3	13.7	0.3	89	86
25.3	13.8	0.2	89	86
26.3	13.8	0.2	89	86
27.3	13.9	0.2	89	86
28.3	14.0	0.1	89	86
29.3	14.0	0.1	88	85
30.3	14.1	0.1	88	85
31.3	14.1	0.0	88	85
32.3	14.2	0.0	89	85
33.3	14.3	0.0	89	85
34.3	14.3	0.0	89	85
35.3	14.4	-0.0	89	85
36.3	14.4	0.0	89	85

Table A-3c, cont.

Depth (m)	Major Amplitude (cm/s)	Minor Amplitude (cm/s)	Inclination (degrees)	Phase (degrees)
37.3	14.5	0.0	89	85
38.3	14.5	0.1	90	85
39.3	14.6	0.1	90	85
40.3	14.6	0.1	91	84.
41.3	14.6	0.2	91	84
42.3	14.6	0.2	92	84
43.3	14.5	0.2	92	84
44.3	14.4	0.3	93	83
45.3	14.3	0.3	94	83
46.3	14.1	0.3	95	82
47.3	13.8	0.3	96	82

Table A-3d. Characteristics of semidiurnal S_2 tidal currents with depth at Site A. Current characteristics were calculated between August and October 2004. A 90-degree inclination is the major axis of the tide aligned parallel to the local axis of the canal. Phase is defined so that the major axis of the tidal ellipse has a positive crosscanal component. A positive minor axis indicates the tidal currents rotate anticlockwise. Depths are calculated using pressure sensors on the Microcat instruments.

Depth (m)	Major Amplitude (cm/s)	Minor Amplitude (cm/s)	Inclination (degrees)	Phase (degrees)
3.3	4.5	-0.3	90	113
4.3	4.7	-0.3	87	117
5.3	4. 6	-0.2	86	117
6.3	4.5	-0.1	87	116
7.3	4.4	-0. 1	89	114
8.3	4.3	0.0	90	113
9.3	4.3	0.1	91	113
10.3	4.3	0.1	92	110
11.3	4.3	0.1	92	110
12.3	4.3	0.1	92	110
13.3	4.4	0.1	91	110
14.3	4.4	0.1	90	109
15.3	4.5	0.1	90	109
16.3	4.6	0.1	90	110
17.3	4.7	0.1	90	109
18.3	4.8	0.0	90	109
19.3	4.9	0.0	89	109
20.3	4.9	0.0	89	109
21.3	5.0	0.1	88	108
22.3	5.0	0. 1	88	108
23.3	5.0	0.1	88	108
24.3	5.0	0.1	88	108
25.3	5.0	0.2	87	107
26.3	5.0	0.2	88	107
27.3	5.0	0.2	88	106
28.3	5.0	0.2	88	106
29.3	5.0	0.1	88	106
30.3	4.9	0.1	88	105
31.3	4.9	0.1	88	106
32.3	4.9	0.0	88	106
33.3	4.9	0.0	88	107
34.3	4.9	-0.0	88	107
35.3	4.9	-0.0	88	107
36.3	4.9	-0.0	89	107

Table A-3d, cont.

Depth (m)	Major Amplitude (cm/s)	Minor Amplitude (cm/s)	Inclination (degrees)	Phase (degrees)
37.3	4.9	-0.0	88	107
38.3	4.9	-0.0	89	106
39.3	4.9	-0.0	90	106
40.3	4.9	-0.0	90	106
41.3	4.9	-0.0	91	105
42.3	4.9	0.0	92	105
43.3	4.9	0.0	93	104
44.3	4.8	0.0	93	104
45.3	4.8	0.0	94	103
46.3	4.7	0.0	95	102
47.3	4.6	0.0	96	102

Table A-4a. Characteristics of diurnal O_1 tidal currents with depth at Site B. Current characteristics were calculated between August and October 2004. 90 degree inclination is the major axis of the tide aligned parallel to the canal. Phase is defined so that the major axis of the tidal ellipse has a positive crosscanal component. A positive minor axis indicates the tidal currents rotate anticlockwise. Depths are calculated using pressure sensors on the Microcat instruments.

Depth (m)	Major Amplitude (cm/s)	Minor Amplitude (cm/s)	Inclination (degrees)	Phase (degrees)
3.9	1.6	0.0	91	347
4.9	2.1	0.1	96	7
5.9	1.9	-0.1	97	6
6.9	1.7	-0.2	98	5
7.9	1.6	-0.3	96	2
8.9	1.5	-0.2	97	359
9.9	1.5	-0.2	101	356
10.9	1.5	-0.2	105	354
11.9	1.4	-0.1	107	354
12.9	1.3	-0.0	110	353
13.9	1.3	0.0	111	355
14.9	1.3	-0.0	111	356
15.9	1.3	-0.1	109	357
16.9	1.4	-0.1	105	358
17.9	1.4	-0.2	103	359
18.9	1.4	-0.2	100	1
19.9	1.4	-0.3	96	2
20.9	1.5	-0.3	93	5
21.9	1.6	-0.3	91	5
22.9	1.6	-0.3	89	6
23.9	1.7	-0.3	88	6
24.9	1.8	-0.3	86	6
25.9	1.8	-0.3	85	6
26.9	1.9	-0.4	82	7
27.9	1.9	-0.4	80	8
28.9	1.9	-0.4	80	7
29.9	2.0	-0.4	80	7
30.9	1.9	-0.4	80	6
31.9	1.9	-0.4	80	3
32.9	1.9	-0.5	82	1
33.9	1.9	-0.4	83	357
34.9	1.9	-0.4	84	354
35.9	1.9	-0.4	85	351
36.9	1.9	-0.3	86	349
37.9	1.8	-0.3	86	346

Table A-4b. Characteristics of diurnal K_1 tidal currents with depth at Site B. Current characteristics were calculated between August and October 2004. A 90-degree inclination is the major axis of the tide aligned parallel to the local axis of the canal. Phase is defined so that the major axis of the tidal ellipse has a positive crosscanal component. A positive minor axis indicates the tidal currents rotate anticlockwise. Depths are calculated using pressure sensors on the Microcat instruments.

Depth (m)	Major Amplitude (cm/s)	Minor Amplitude (cm/s)	Inclination (degrees)	Phase (degrees)
3.9	1.9	-0.1	100	24
4.9	2.1	-0.1	104	32
5.9	2.3	-0.2	103	23
6.9	2.3	-0.1	102	17
7.9	2.3	-0.0	101	13
8.9	2.4	-0.0	102	10
9.9	2.4	0.0	101	8
10.9	2.4	0	100	6
11.9	2.4	-0.0	100	7
12.9	2.4	-0.1	99	8
13.9	2.4	-0.0	96	9
14.9	2.5	0.0	95	12
15.9	2.5	0.0	94	14
16.9	2.6	-0.0	94	16
17.9	2.6	-0.1	93	17
18.9	2.6	-0.2	92	19
19.9	2.7	-0.3	91	20
20.9	2.8	-0.4	91	22
21.9	2.8	-0.4	90	22
22.9	2.9	-0.4	89	24
23.9	2.9	-0.4	88	25
24.9	2.9	-0.4	86	25
25.9	3.0	-0.4	86	25
26.9	3.0	-0.4	85	25
27.9	3.0	-0.4	84	24
28.9	3.1	-0.4	83	22
29.9	3.1	-0.4	82	9
30.9	3.0	-0.4	82	6
31.9	3.0	-0.5	81	4
32.9	3.1	-0.5	82	2
33.9	3.1	-0.5	83	9
34.9	3.0	-0.5	83	7
35.9	2.9	-0.5	84	5
36.9	2.8	-0.4	86	3
37.9	2.6	-0.3	87	1

Table A-4c. Characteristics of semidiurnal M_2 tidal currents with depth at Site B. Current characteristics were calculated between August and October 2004. A 90-degree inclination is the major axis of the tide aligned parallel to the local axis of the canal. Phase is defined so that the major axis of the tidal ellipse has a positive crosscanal component. A positive minor axis indicates the tidal currents rotate anticlockwise. Depths are calculated using pressure sensors on the Microcat instruments.

Depth (m)	Major Amplitude (cm/s)	Minor Amplitude (cm/s)	Inclination (degrees)	Phase (degrees)
3.9	8.3	-0.3	98	95
4.9	9.1	-0.1	101	99
5.9	9.0	-0.1	102	96
6.9	8.8	0.1	103	95
7.9	8.6	0.2	103	96
8.9	8.4	0.4	103	97
9.9	8.2	0.6	103	99
10.9	7.9	0.8	102	100
11.9	7.7	0.9	101	101
12.9	7.6	0.9	100	102
13.9	7.5	0.9	99	103
14.9	7.4	0.7	98	104
15.9	7.4	0.6	96	105
16.9	7.5	0.3	95	106
17.9	7.5	0.1	93	107
18.9	7.6	-0.2	92	107
19.9	7.7	-0.4	90	108
20.9	7.9	-0.7	89	109
21.9	8.0	-0.9	89	110
22.9	8.0	-1.1	88	110
23.9	8.1	-1.3	88	111
24.9	8.1	-1.4	88	111
25.9	8.1	-1.5	89	111
26.9	8.1	-1.6	89	111
27.9	8.0	-1.6	90	111
28.9	7.9	-1.6	91	111
29.9	7.9	1.6	92	110
30.9	7.8	1.5	92	110
31.9	7.7	1.4	93	109
32.9	7.5	1.2	93	108
33.9	7.4	0.9	93	107
34.9	7. 2	0.7	94	105
35.9	6.9	0.5	94	103
36.9	6.7	0.4	94	101
37.9	6.4	0.1	93	98

Table A-4d. Characteristics of semidiurnal S_2 tidal currents with depth at Site B. Current characteristics were calculated between August and October 2004. A 90-degree inclination is the major axis of the tide aligned parallel to the local axis of the canal. Phase is defined so that the major axis of the tidal ellipse has a positive crosscanal component. A positive minor axis indicates the tidal currents rotate anticlockwise. Depths are calculated using pressure sensors on the Microcat instruments.

Depth (m)	Major Amplitude (cm/s)	Minor Amplitude (cm/s)	Inclination (degrees)	Phase (degrees)
3.9	2. 7	0.0	103	116
4.9	3.0	0.1	104	119
5.9	3.2	0.1	105	113
6.9	3.3	0.1	105	113
7.9	3.2	0.2	105	116
8.9	3.1	0.2	104	118
9.9	2.9	0.3	103	121
10.9	2.7	0.4	103	123
11.9	2.6	0.4	102	125
12.9	2.6	0.4	100	126
13.9	2.5	0.3	97	126
14.9	2.5	0.2	95	126
15.9	2.5	0.1	93	128
16.9	2.5	-0.0	92	129
17.9	2.6	-0.1	92	131
18.9	2.6	-0.2	92	134
19.9	2.7	-0.3	93	135
20.9	2.7	-0.4	93	137
21.9	2.7	-0.4	93	138
22.9	2.8	-0.4	94	150
23.9	2.8	-0.4	95	139
24.9	2.7	-0.4	96	139
25.9	2.6	-0.5	98	138
26.9	2.5	-0.5	100	137
27.9	2.5	-0.5	101	135
28.9	2.4	-0.5	101	134
29.9	2.4	-0.5	101	133
30.9	2.4	-0.5	102	132
31.9	2.4	-0.5	102	130
32.9	2.4	-0.4	102	128
33.9	2.3	-0.4	100	126
34.9	2.3	-0.3	98	123
35.9	2.2	-0.2	95	121
36.9	2.1	-0.1	91	117
37.9	2.0	-0.1	89	113